The Development of a Pulse-Spread Technique to Analyze the Directionality of Neurofilament Transport in Axons

Honors Research Thesis

Presented in partial fulfillment of the requirements for graduation *with honors research distinction* in Biology in the undergraduate colleges of The Ohio State University

By

Amrita Mukhopadhyay

The Ohio State University
May 2012

Project Advisor: Dr. Anthony Brown, Department of Neuroscience

Acknowledgements

I would like to thank Dr. Brown for giving me the opportunity to conduct research in his lab, awarding me with financial support, and providing with me his time, invaluable guidance, and encouragement. I would also like to thank Paula Monsma for her time and patience in teaching me instrumental lab techniques. Additionally, I would like to thank all of the members of the Brown Lab for welcoming me, creating a wonderful atmosphere to work in, and teaching me how to think like a scientist. Finally, I would like to thank my friends and family for all of their support throughout my undergraduate career.

Statement of Contribution

Amrita Mukhopadhyay did all of the imaging, analysis, and figure preparation for this thesis. She also did most of the transfection and staining prior to imaging. During the summer, Amrita established some cell cultures, but during the academic year, rat DRG cultures were established by Paula Monsma, a research assistant in the lab. Paula also conducted some of the transfection, staining, and DNA preparation protocols.

Table of Contents

Contents

Chapter 1: Introduction

Background

Roles of Neurofilaments

Cells of the nervous system are morphologically unique compared to other cell types due to the presence of neuronal processes. This places heavy demands on the cytoskeletal system, especially in the axon, which is of special interest due to its integral role in neuronal signaling. Of the three main classes of cytoskeletal proteins (microtubules, microfilaments and intermediate filaments), intermediate filaments are the most prominent in the axon (Gotow, 2011; Perrot, 2009). These intermediate filaments, called neurofilaments in the neuron, are polymer chains consisting of different protein types, including light (NFL), medium (NFM), heavy (NFH) and α-internexin in the central nervous system, in addition to peripherin in the peripheral nervous system (Beaulieu, 1999; Yan, 2007; Yuan, 2006).

Neurofilaments play the important role of increasing axon caliber, thereby increasing conduction velocity, or the velocity of neuronal signaling (Perrot, 2008). They are the most abundant structure in large axons and occupy almost all of the axoplasm (Gotow, 2011; Perrot, 2009). The abundance and organized nature of neurofilaments can be observed in Figure 1.1, which shows an axonal cross-section.

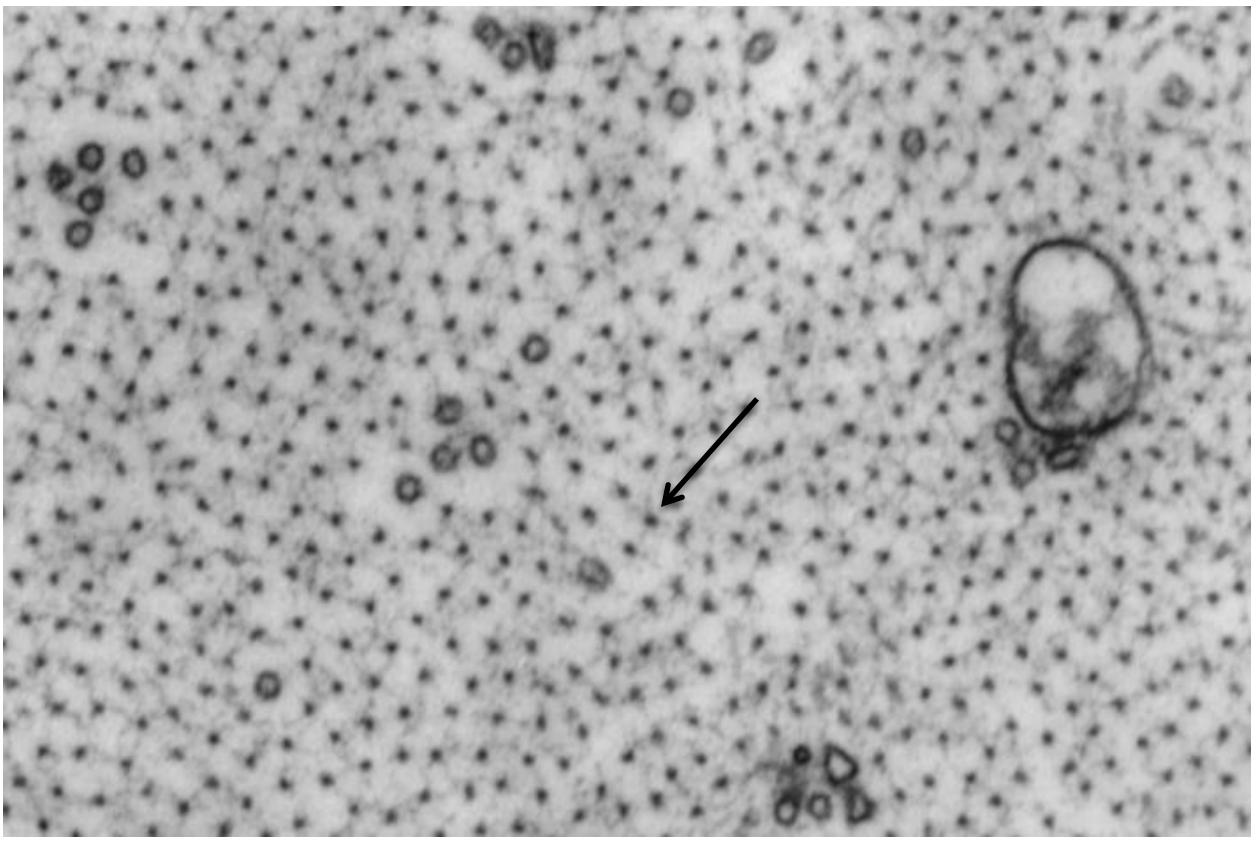

Figure 1.1: Cross-section of an axon with many neurofilaments. The black arrow is pointing to a neurofilament.

Accumulation of neurofilaments, resulting in increased axon caliber, can occur in both healthy and diseased neurons. One example of healthy neurofilament accumulation involves myelination, where non-neuronal cells (Schwann cell or oligodendrocyte) wrap around the axon, creating an electric insulation that increases conduction velocity. This process occurs in conjunction with a marked increase in neurofilament content and axon caliber, which also increases conduction velocity (de Waegh, 1992; Windebank, 1985). Figure 1.2 shows a cross-section of a myelinated axon next to an unmyelinated axon. The dark band indicated by the white triangle (right) is the myelin sheath made up of multiple layers of Schwann cell membrane. Note the large size of the myelinated axon compared to the unmyelinated axon (left white triangle) as well as the high number of neurofilmants (black arrow) present.

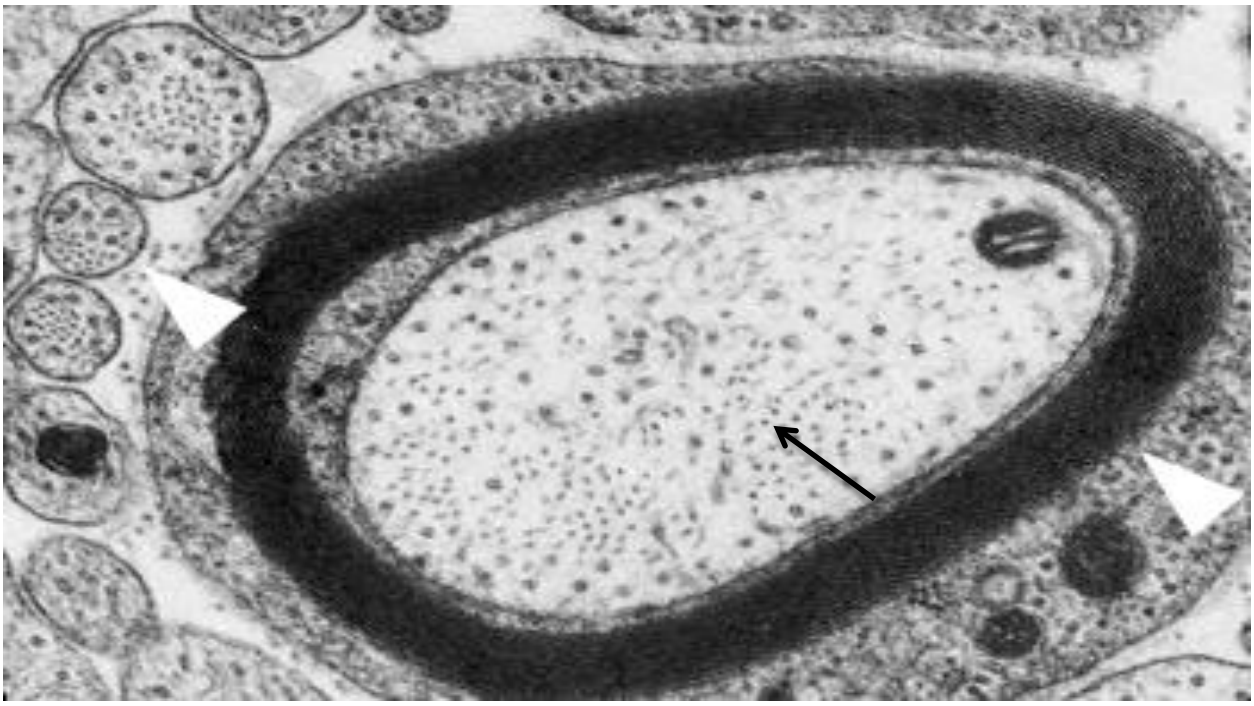

Figure 1.2: Cross-section of myelinated and unmyelinated axons. White triangles designate the myelin sheath (right) and an unmyelinated axon (left). The black arrow indicates a neurofilament. Adapted from Eldridge, 1998.

Accumulation of neurofilaments may also be pathological and has been associated with several neurodegenerative diseases, including amyotrphic lateral sclerosis (ALS), Alzheimer's disease (AD), Parkinson' disease (PD), dementia with Lewy bodies, Charcot-Marie-Tooth disease (CMT), giant axonal neuropathy (GAN), neuronal intermediate filament inclusion disease (NIFID), diabetic neuropathy, spinal muscular dystrophy and hereditary spastic parapalegia (Perrot, 2009; Barry, 2007; De Vos, 2008; Julien 1997). In many of these diseases, neurofilament accumulation results in large swellings within the axon (Perrot, 2009; Julien 1997). While neurofilament accumulation could be a pathological outcome, recent studies have suggested that it may be a cause of pathology as well (Perrot, 2009). Figure 1.3 depicts this model of neurodegeneration, with neurofilament accumulation resulting in axonal atrophy.

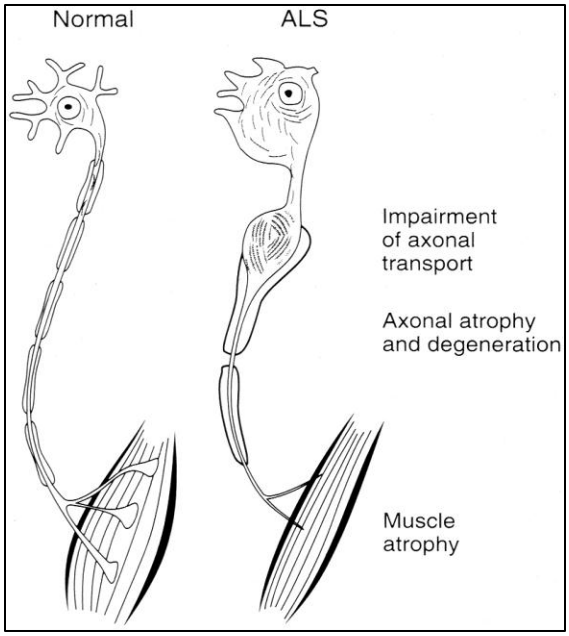

Figure 1.3: Neurodegenerartive model depicting axonal blockage by neurofilaments, resulting in atrophy. Adapted from Julien, 1997.

Axonal Transport of Neurofilaments

Whether in healthy myelinating cells or in diseased neurons, mechanisms of neurofilament accumulation are not well understood. Studies have suggested that accumulation could be caused by alterations in axonal transport (Barry, 2007; De Vos, 2008; Perlson, 2010; Julien, 1997). Neurofilaments are thought to be transported via "stop-and-go" slow axonal transport, which is bidirectional (Glass, 1991; Watson, 1993) and consists of rapid bursts of movement with intermittent pauses (Brown, 2000, 2005, 2009; Li, 2012). The kinetic profiles depicted in Figure 1.4 demonstrate the nature of this movement.

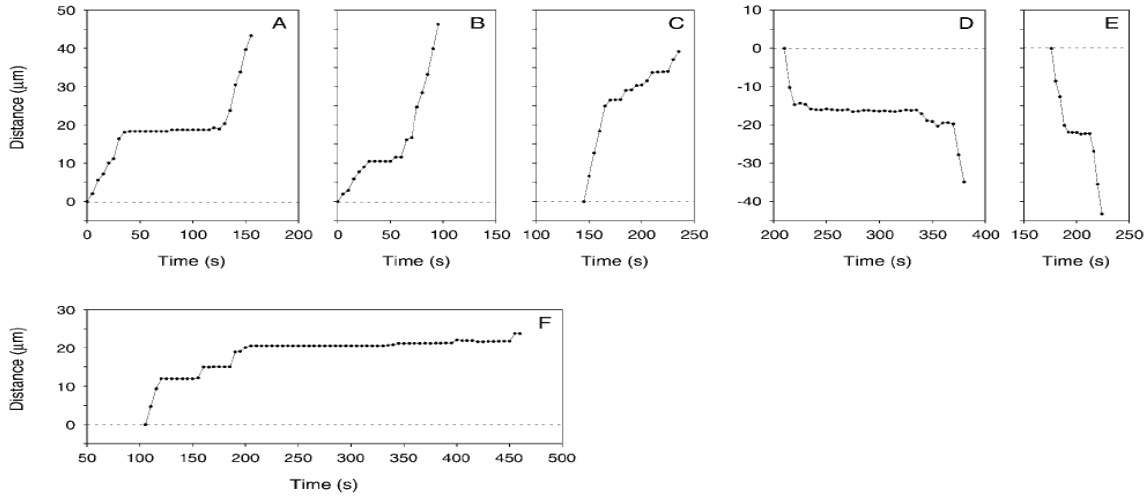

Figure 1.4: Kinetic profiles demonstrating "stop-and-go" movement of neurofilaments in axons. Each point represents the location of a neurofilament at one point in time. Adapted from Wang, 2001.

The current model to explain neurofilament movement involves the concept of microtubule tracks. Many other cellular entities, such as mRNAs, proteins and vesicles, travel along cytoskeletal protein polymers called microtubules (Hirokawa, 2010). It is thought that neurofilaments may have "on-track" and "off-track" states (Li, 2012). In the "on-track" states, neurofilaments are associated with the microtubule track and are moving or pause for short amounts of time, while in the "off-track" states, they remain paused for hours. Figure 1.5 depicts a cartoon of a neurofilament moving on and off of the microtubule track alongside a schematic of the six possible "on-track" and "off-track" states.

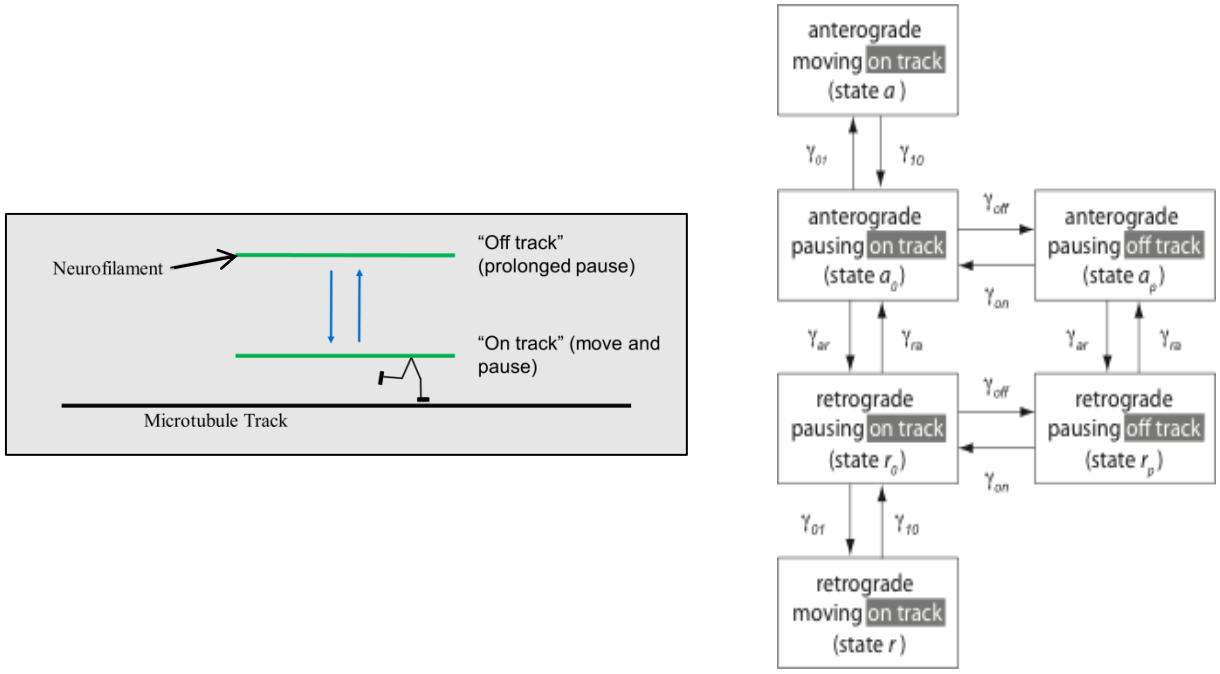

Figure 1.5: Cartoon of a neurofilament moving betwwn "on-track" and "off-track" alongside a schematic of "on-track" and "off-track" states in neurofilament transport. Adapted from Yi, 2012.

Neurofilament content is determined by residence time in the axon, which is determined by the average velocity. Thus, accumulation would be caused by a local decrease in neurofilament velocity occurring through two possible mechanisms—an increased frequency of pausing ("on-track"→ "off-track"), or an increased frequency of reversal (anterograde ↔ retrograde). Thus, the bidirectional nature of neurofilament transport is important to consider. Specifically, examination of the ratio between anterograde (away from cell body) and retrograde (towards cell body) transport is necessary, as this ratio must be tightly regulated within the cell to control neurofilament content (Jung, 2009).

Study of Neurofilament Transport Directionality

Natural Gap Technique

Previous study of the ratio between anterograde and retrograde transport found 83% of neurofilaments traveling in the anterograde direction (Wang, 2000). This was observed through a "natural gap technique," which has inherent limitations. This technique exploits the presence of gaps where no

neurofilaments are apparent within the axon. The gaps occur naturally, are thought to have no functional significance, and occur only in very thin axons with low neurofilament content, such as those from the superior cervical ganglia. Figure 1.6 depicts a schematic of the natural gap technique with fluorescently-tagged neurofilament proteins shown in green. Neurofilament transport can be observed within the gaps.

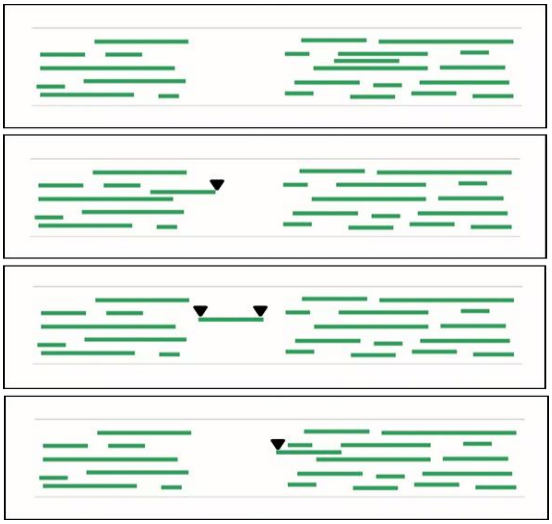

Figure 1.6: Schematic of "natural gap technique" with fluorescently-tagged neurofilaments represented in green.

Figure 1.7 shows multiple frames from a time-lapse movie using this technique. Rat neurofilament protein M (rNFM) is tagged with green fluorescent protein (GFP) through transfection with a GFP-rNFM construct.

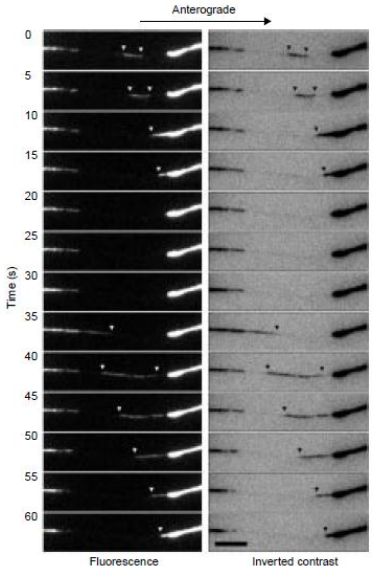

Figure 1.7: Images from a time-lapse movie using the "natural gap technique." Neurons from superior cervical ganglia of rats were transfected with green fluorescent protein-tagged neurofilament protien M (GFP-rNFM). Scale bar = 5 µm. Adapted from Wang, 2000.

While an anterograde bias was detected in these axons, it is important to note that the sample observed was skewed, as only neurofilaments in naturally occurring gaps could be analyzed. This is because fluorescently labeled mobile neurofilaments outside of the gap would not be distinguishable from fluorescently labeled non-mobile ones. Another limitation of the natural gap technique lies in its small sample size with respect to the number of neurofilaments observed per axon—individual neurofilaments are examined as opposed to populations of neurofilaments. Additionally, only neurons with low neurofilament content, such as those from the superior cervical ganglia, present with naturally occurring gaps, and therefore, this technique is limited to these types of neurons.

A similar method involving photobleaching (or the over-excitation of a fluorescent protein so it no longer fluoresces) was later employed for the study of neurofilament transport (Wang, 2001). This study reported 67% of neurofilaments moving in the anterograde direction, compared to the earlier observation of 83%. Essentially, photobleaching was used to lower the fluorescence in a region of the axon to create a "virtual" gap. Movement of neurofilaments through this gap was observed, similar to the natural gap technique. While photobleaching allows for the monitoring of neurofilaments outside of naturally occurring gaps, other limitations remain. Because both the natural gap and the photobleaching techniques rely on the observation of single neurofilaments through a specific axonal region, the kinetics of a population of neurofilaments over a longer period of time (minutes instead of seconds) cannot be discerned using these methods.

The Pulse-Escape Technique

In order to examine the transport of neurofilament populations over a longer period of time, a fluorescence photoactivation method can be employed. In this type of method, neurofilament proteins are tagged with photoactivatable (PA) fluorescent proteins, which only fluoresce after activation with a specific wavelength of light. The "pulse-escape" technique is a type of fluorescence photoactivation method that was developed for the study of neurofilament pausing behavior (Trivedi, 2007). Figure 1.8 depicts a schematic of this technique, with unactivated PA-GFP tagged rat neurofilament protein M (PA-GFP-rNFM) represented in gray and activated PA-GFP-rNFM represented in green. A specific region of the axon can be activated through a "pulse" of violet light (yellow box). The rate of neurofilament dispersal, or "escape," from the activated region can then be studied by quantification of decrease in fluorescence of the activated region.

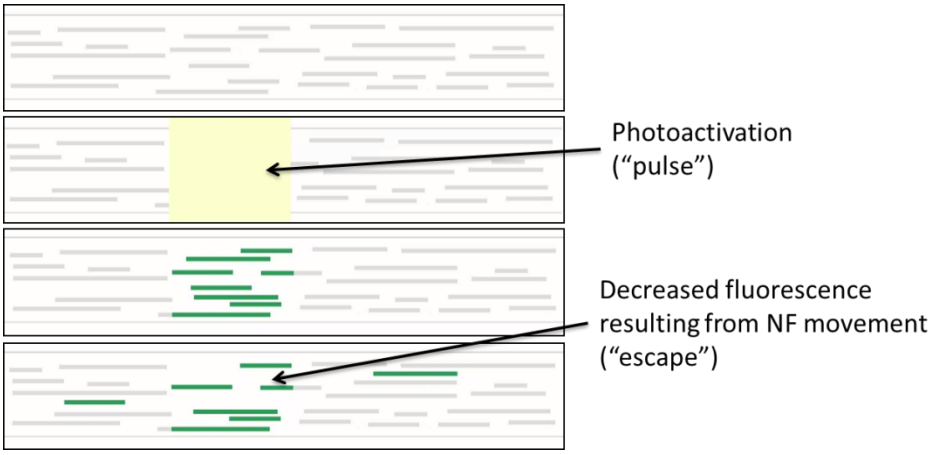

Figure 1.8: Schematic of the pulse-escape techniqe. Adapted from Trivedi, 2007.

While this technique was originally conducted in SCG cells, there is no reason why it cannot be employed using neurons with thicker axons, such as those found in dorsal root ganglia (DRG), which contain tens to hundreds of neurofilaments per axonal cross-section. Doing so would allow for the monitoring of neurofilament populations. Additionally, even though the pulse-escape technique was originally designed for the study of pausing behavior, modification could allow for the study of transport directionality by measuring fluorescence in the anterograde and retrograde directions from the activated region. Thus, the "spread" of neurofilaments from the activated region could be characterized. This thesis discusses the modification of the pulse-escape technique into the "pulse-spread" technique for examining neurofilament transport directionality in DRG cultured neurons.

End-binding (EB) Proteins

In order to determine which direction of movement is anterograde and which is retrograde, the proximal and distal ends of an axon must be known. Previous studies of neurofilament transport directionality in SCG cells designated this by locating neuronal cell bodies, which are at the proximal end of axons (Wang, 2001). DRG cultures, along with other culture types, are too dense to accurately trace axons back to their cell bodies. Thus, alternate methods of determining directionality are needed.

One method of designating proximal and distal ends of axons involves microtubules. As previously mentioned, microtubules are a class of cytoskeletal proteins distinct from neurofilaments. They are made up of α and β-tubulin protein heterodimers, and are polar in structure, with fast-growing plus-ends and slow-growing minus-ends (Maurer, 2012; Stepanova, 2010; Akhmanova, 2010; Montenegro, 2010; Galjart, 2010; Stepanova, 2003). Microtubules exist in all eukaryotic cells, but exhibit a unique unipolar arrangement in axons where all plus-ends point in the anterograde direction (Stepanova, 2010).

The plus-ends of microtubules are dynamic in that they are constantly growing and shrinking (Maurer, 2012; Stepanova, 2010; Akhmanova, 2010; Montenegro, 2010; Galjart, 2010; Stepanova, 2003). During growth, GTP-bound heterodimers congregate at the plus-end. As the microtubule continues to grow, GTP is hydrolyzed to GDP. This hydrolysis is delayed after assembly, resulting in the formation of a GTP cap. Several proteins, referred to as plus-end tracking proteins (+TIPs), cluster around the plus-end to assist with microtubule dynamics and cellular interactions. These proteins are thought to bind to the

GTP cap. When the cap is lost, GDP-bound heterodimers, which have less affinity to each other, are exposed and curve away from the microtubules. During this disassembly, the microtubule is shrinking and +TIPs are no longer associated with it. Figure 1.9 shows a schematic of a growing and shrinking microtubule with a specific class of +TIPs called end-binding (EB) protein.

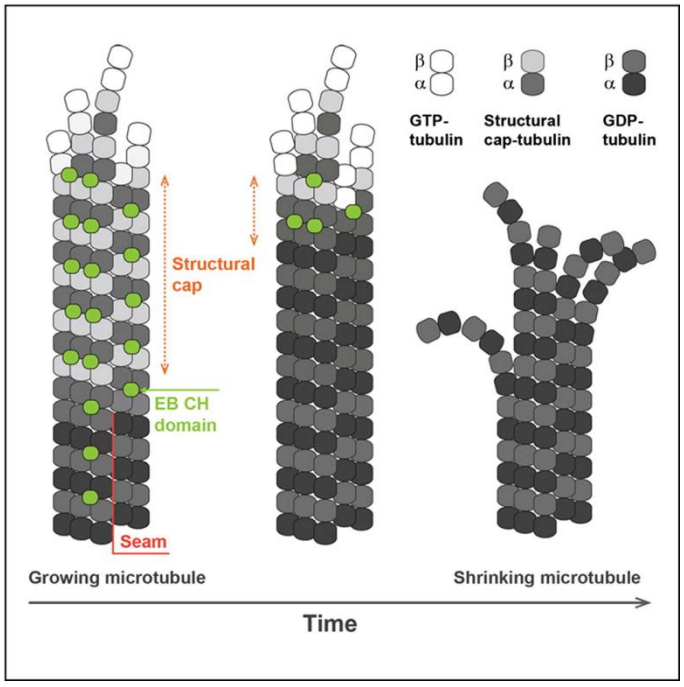

Figure 1.9: Schematic of a growing and shrinking microtubule. End-binding (EB) proteins are shown in green, and only cluster around the microtubule end during growth. Adapted from Maurer, 2012.

Because +TIPs, such as EB proteins, only congregate at growing microtubule ends, fluorescent labeling of these structures can allow for visualization of growing ends, but not shrinking ones (Stepanova, 2010). Therefore, since microtubules only grow in the anterograde direction in axons, monitoring of fluorescently-tagged +TIPs can reveal an axon's proximal and distal ends (Stepanova, 2010). In this thesis, exploitation of EB protein behavior is combined with the previously discussed fluorescence photoactivation methodology, resulting in the "pulse-spread" technique.

Chapter 2: Materials and Methods

Cell Culture

Non-Myelinating DRG Cultures

Primary fetal rat dorsal root ganglia (DRG) co-ultures were established using the rapid method for culturing embryonic neuron-glia cell cocultures (Svenningson et al., 2003). Sprague-Dawley pregnant female rats were obtained from Harlan Laboratories (Indianapolis, IN). Caesarean sections were performed at 16.5 days in utero. Embryos were eviscerated, the spinal cord removed, and dorsal root ganglia (DRG) were transferred to cold L15 medium (Invitrogen).

DRGs were rinsed in phosphate buffered saline (PBS; Invitrogen, Carlsbad, CA) and dissociated in PBS containing 3.5 mg/ml trypsin (Worthington Biochemical Corp., Lakewood, NJ) at 37°C for 30 min. To halt trypsin activity, PBS containing 25% fetal bovine serum (FBS; Invitrogen) was used. Ganglia were rinsed in L15 medium supplemented with 0.5 mg/ml bovine serum albumin (BSA; Calbiochem) and triturated. Cells were plated in sterilized glass-bottomed dishes coated with poly-lysine (Sigma) and Phenol Red-free Matrigel (BD Biosciences).

Cells were plated at approximately 60 cells/mm² in NbActiv4 medium (Brain Bits, LLC) supplemented with 100 ng/ml nerve growth factor (NGF; BD Biosciences) and maintained at 37°C/5% CO_2. For studies specified, NbActiv medium contained phenol red pH indicator. After the first six days, the medium was replaced. Half of the medium was replaced every two to three days, with a full medium replacement every seven days. Cultures were transfected after 2-3 weeks *in vitro*.

Myelinating DRG Cultures

For the older, myelinating cultures discussed in Chapter 4, cells were plated in Neurobasal medium (Gibco) supplemented with 20 mM L-glutamine (Sigma), 2% B-27 (Gibco), and 50 ng/ml NGF. After the first six days of culture, medium was replaced as before, but new medium was supplemented with Matrigel at a 1:100 ratio. Two days later, half of the medium was replaced with culturing medium, which did not contain Matrigel, but contained freshly dissolved ascorbic acid (Sigma) at 50 µg/ml. All subsequent media replacements were made at the same schedule as mentioned before using media supplemented with ascorbic acid. Cultures were transfected after 3-4 weeks *in vitro*.

For studies comparing neurotrophin-3 (NT-3) and NGF (Chapter 5), cells were plated in NbActive medium supplemented with either 25 ng/ml NT-3 (PeproTech) or 50 ng/ml NGF at 120 cells/mm^2 and 60 cells/mm^2, respectively (there are less NT-3 dependent cells in DRG neurons). Culturing protocol was identical to the older, myelinating cultures. Cultures were imaged after 28 days *in vitro*.

Cloning

EB3-mCherry

The EB3-mCherry plasmid construct was a generous gift from Dr. Peter Baas at Drexel University, who received it from Dr. Vic Small at the Institute for Molecular Biotechnology (Vienna, Austria). The construct was originally created by replacement of GFP with mCherry into pEGFP-N1-EB3 via BamHI and BsrGI sites (Efimov et al., 2008). Figure 2.1 shows the plasmid parent vector used.

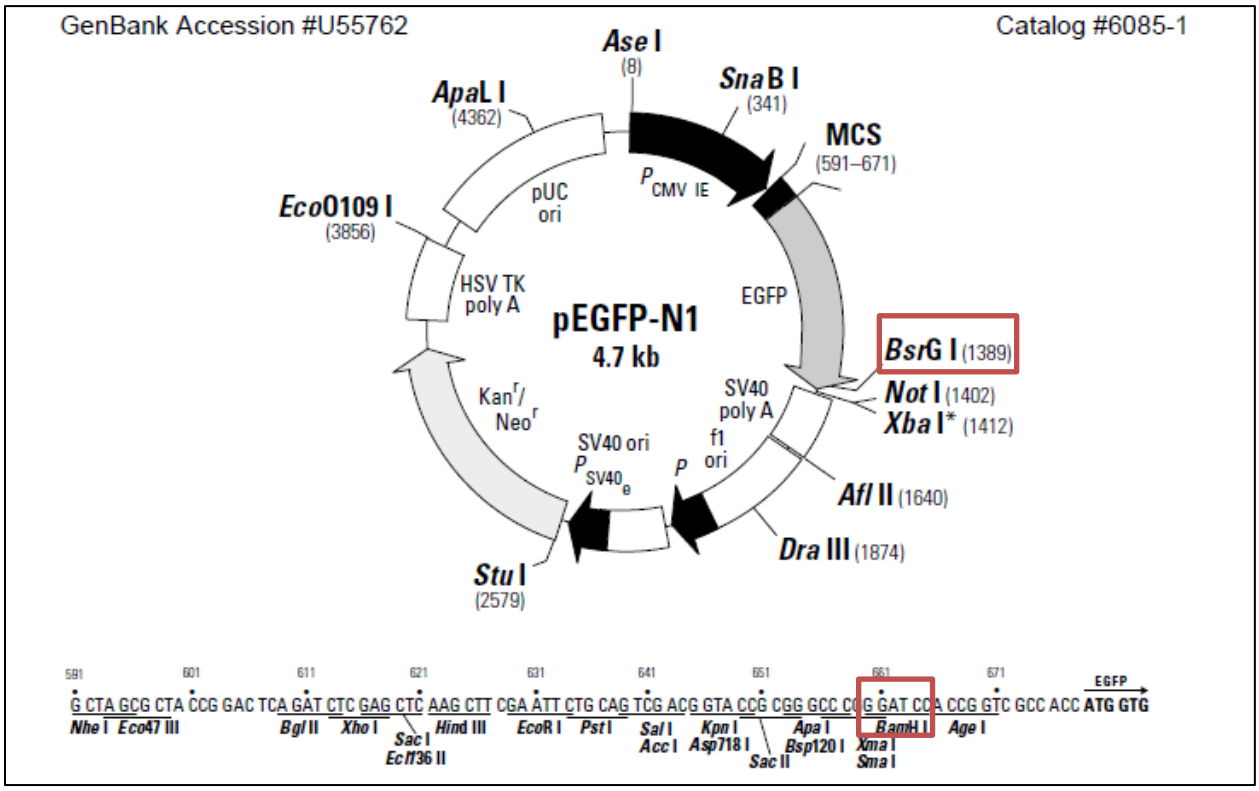

Figure 2.1: Restriction map and multiple cloning site (MCS) of pEGFP-N1 plasmid parent vector used for EB3-mCherry construct. Red boxes indicate the restriction sites used. Adapted from GenBank catalog.

EB1-YFP

The EB1-YFP plasmid construct was a generous gift from Dr. Chen Gu at The Ohio State University, and was originally constructed via insertion of the EB1 coding sequence into pEYFP-N1 between BglII and HindIII sites (Gu et al., 2006).

PA-GFP-rNFM

The PA-GFP-rNFM plasmid construct was previously created by excising complementary DNA encoding for rat NFM from the EGFP-rNFM (the "r" prefix in "rNFM" indicates rat) construct and inserting it into the PA-GFP-C1 vector via BamHI and KpnI (Trivedi, 2007).

Transfection

Cells were transfected 5-7 days before imaging using Lipofectamine LTX and Plus reagent (Invitrogen). Prior to Lipofection, Opti-MEM I (Gibco) was pre-equilibrated at 37°C/5%CO_2 for 30 min, the appropriate amounts of DNA and Lipofectamine reagent (see Table 2.1) were brought to room temperature, and culture medium was changed for cells at 80% confluency. To the DNA and Lipofectamine separately, 250 µl of Opti-MEM was added and allowed to incubate for 5 min at room temperature. The mixture with DNA was then added to the mixture with Lipofectamine, allowed to incubate at 37°C/5%CO_2 for 20 min, and added to the cells. The medium was replaced after 18-24 hours.

Table 2.1: DNA and Lipofectamine reagent amounts used for transfection.

	Age at transfection	DNA	Lipofectamine
Ch. 3	14-21 days *in vitro*	5 µg EB3-mCherry or 5 µg EB1-YFP	20 µl
Ch. 4	Young cultures: 14-21 days *in vitro* Old cultures: 21-28 days *in vitro*	2 µg EB3-mCherry and 5 µg PA-GFP-rNFM	21 µl

Live Cell Imaging

Imaging of Comet Movement

To image EB1-YFP and EB3-mCherry comets, cultures were observed 5-7 days after transfection by epifluorescence microscopy using a Nikon TE2000 microscope with a 40x Plan Apo 1.0NA objective, and EYFP (Chroma #41028) or ET-mCherry (Chroma #49008) filter cube, respectively. An observation medium of Hibernate EB LF (BrainBits, Springfield, IL) supplemented with 100 ng/ml NGF was used, and dimethylpolysiloxane fluid (Sigma, 5 centistokes) was floated over top of the medium to prevent evaporation. For cultures that exhibited higher levels of expression, neutral density filters were used to attenuate the exciting light from the mercury lamp in 4-fold. Images were acquired using the Micromax 512 BFT camera (Roper Scientific, Inc.) with one second exposures at two second intervals for two minutes.

Pulse-Spread Imaging

For pulse-spread imaging, cultures were observed 5-7 days after transfection by epifluorescence microscopy using a Nikon Eclipse TiE inverted microscope with a 40x Plan Apo 1.0NA objective, ET-mCherry (Chroma #49008) and ET-GFP (Chroma #49002) filter cubes. To ensure all axons imaged were unmyelinated, older cultures were stained using FluoroMyelin™ red fluorescent myelin stain (Invitrogen), which was combined with observation medium in a 1:300 ratio and added to cover cells two hours prior to imaging. An observation medium of Hibernate EB LF (BrainBits, Springfield, IL) supplemented with 50-100 ng/ml NGF was used, and dimethylpolysiloxane fluid (Sigma, 5 centistokes) was floated over top of the medium to prevent evaporation during imaging.

Pulse-spread involved two phases of imaging. First, comets of an axon were observed as described above, and then analyzed through kymograph generation (as described in Chapter 3). After proximal and distal ends of the axon were designated from kymographs, a segment of the axon that was in focus for about 30 µm in length was positioned in the center of the field of view and images were taken with

both the ET-mCherry and ET-GFP filter cubes. A region of approx. 5 µm in length was activated using a mosaic micro-mirror array digital diaphragm (Phototonic Instruments, Inc.) and a custom filter cube (Chroma set #C107375) that allowed only for the passage of violet light, as previously described (Trivedi, 2007). Images were taken with a CoolSnap HQ camera (Photometrics) using both the ET-mCherry and the ET-GFP filter cubes at 0, 10, 20, and 30 min. The ET-mCherry images were used to ensure that the axon did not drift out of focus. If this were the case, the microscope was re-focused prior to taking the image with the ET-GFP filter cube. ET-mCherry images were taken at one second exposures with neutral density filters to attenuate the exciting light if expression level was high. ET-GFP images were taken at two second exposure, and always used a neutral density filter that attenuated exciting light from the mercury lamp in 4-fold.

Imaging of Axon Caliber

To image the caliber of myelinated axons, cultures were observed 21 days *in vitro* by epifluorescence microscopy using a Nikon Eclipse TiE inverted microscope with a 40x Plan Apo 1.0NA objective and a custom FluoroMyelin™ red (Chroma set #C-124896) filter cube. Two hours prior to imaging, cultures were stained using FluoroMyelin™ red (FMR) fluorescent myelin stain (Invitrogen), which was combined with observation medium in a 1:300 ratio and added to cover cells two hours prior to imaging. An observation medium of Hibernate EB LF (BrainBits, Springfield, IL) supplemented with either 50 ng/ml NGF or 25 ng/ml NT-3 was used, and dimethylpolysiloxane fluid (Sigma, 5 centistokes) was floated over top of the medium to prevent evaporation. Images were taken at one second exposures using the CoolSnap HQ camera, FMR filter cube, and a neutral density filter that attenuated exciting light from the mercury lamp by 10-fold.

Imaging Analysis

Analysis of Comet Movement

Movement of comets was analyzed through the creation of kymographs. These were generated using the MetaMorph™ imaging software to convert time-lapsed movies into fluorescence vs. time images. A line was drawn along the axon, and the maximum fluorescent intensity across the width of the axon for each pixel in length was used to generate a kymograph image composite (see Chapter 3 for more details). Kymographs were assessed for quality based on the number of comets and the unidirectionality of their movement. The kymograph quality was then correlated with axon width. To measure this, a representative line was drawn perpendicular to the axon, and an intensity profile was generated. The profiles were bell-shaped and displayed a single peak with points of inflection at each end where the background intensity met the axon intensity. The distance between the two points of inflection was recorded as the axon width.

Pulse-Spread Analysis

Using MetaMorph™ imaging software, five different regions were drawn along the axon. The center region encompassed the activated region using the ET-GFP image taken 0 min after activation. The length of this region was set at the point of inflection between activated intensity and unactivated

intensity using the linescan tool. Contiguous regions of identical length were drawn on each side of the center region using the images taken with the ET-mCherry cube. Figure 2.2 shows a schematic of the five regions drawn. The widths of all regions were set at the point of inflection between background intensity and axon intensity in ET-mCherry images using the linescan tool. Background regions were drawn on either side of the axon in very close proximity to the axonal regions, but not overlapping. The integrated intensity, average intensity, area, length and elapsed time from ET-GFP images were recorded for each region at each time point.

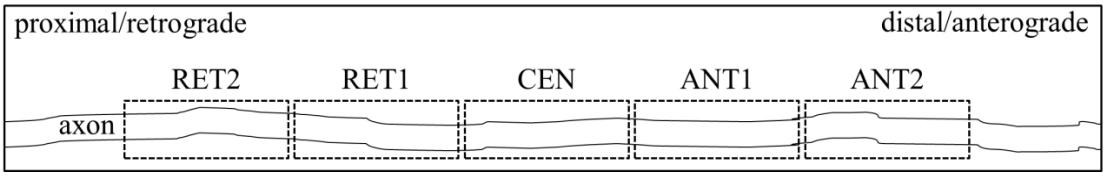

Figure 2.2: Schematic of regions drawn for pulse-spread analysis. CEN is the activated region and was drawn using the ET-GFP image taken immediately after activation. The flanking regions were drawn using the ET-mCherry images.

Several corrections were made. To correct for background intensity, the average intensity per pixel was calculated for the background regions and subtracted accordingly from the axonal regions. To correct for intrinsic autofluorescence of the axon, the background corrected intensity from the image taken prior to activation was subtracted from all other time points. Finally, to correct for photobleaching with neutral density attenuation by 4-fold, values were divided by the bleach correction factor. Bleach calibration was conducted by Paula Monsma in the Brown Lab, resulting in equation 2.1 to calculate the bleach correction factor (c) as a function of number of images taken (n).

Equation 2.1

$$c = e^{-0.010866\,(n-1)}$$

Corrected integrated intensity values for each axonal region at each time point were then normalized to the corrected integrated intensity at activation. Time was determined by subtracting the elapsed time for the image at 0 min after activation from elapsed time for images taken for the other time points.

Measurement of Axon Caliber

Axon caliber was measured using the MetaMorph™ imaging software linescan tool. A line was drawn perpendicular to the axon to generate the linescan profile of the myelin. Distances were measured at half of the peak fluorescent intensity, with “outside” measurements of the outer edges of the myelin sheath, and “inside” measurements of the inner edges of the myelin sheath (see Chapter 5 for more details).

Chapter 3: Designating Directionality

Introduction

The previously established "pulse-escape" technique is a fluorescent photoactivation method allowing for visualization of neurofilament dispersal from a specific segment of axon (Trivedi, 2007). The purpose of this thesis is to discuss a method of modifying this technique in order to resolve the directionality of this dispersal. Previous studies on neurofilament transport directionality in superior cervical ganglia (SCG) cells designated the proximal and distal ends of an axon using the location of the cell body (proximal is towards the cell body) (Wang, 2000). However, dorsal root ganglia (DRG) neuron-glial co-cultures are highly dense with very long neurons, making it difficult to trace a single axon to its cell body. For this reason, we sought to exploit the binding characteristics of the end-binding (EB) protein family to determine the anterograde and retrograde directions for each axon.

As previously discussed, end-binding proteins cluster around growing tips of microtubules, but not around shrinking tips. Since microtubules only orient in the anterograde direction in axons, and therefore only grow in this direction, fluorescently tagged EB proteins can help distinguish directionality. In this set of experiments, the efficacy of the EB3-mCherry (mCherry-tagged EB protein 3) construct is studied in DRG neuron-glial co-cultures. Once efficacy is established, this construct can be used to designate the anterograde direction of an axon prior to fluorescent photoactivation to determine neurofilament transport directionality.

Kymograph Generation

One week after transfection with the EB3-mCherry construct, DRG cells were imaged using epifluorescence microscopy. Images were captured every 2 sec with 1 sec exposure to generate movies 1-2 min in length. Clusters of EB3-mCherry protein around the growing tip of the microtubule appeared as regions of intense fluorescence, or "comets." These comets have been shown to almost always move in the anterograde direction (Stepanova, 2010; Wang, 2010).

Figure 3.1 shows three frames from a movie, in which comets were clearly visible and moving from left to right. The arrows designate the location of four different comets at each timepoint. All of the comets were moving in the same direction, signifying that direction as distal (anterograde). It is important to note that the clarity of comets in this axon was an anomaly. In general, comets were not clearly visible in a movie because of the high amounts of diffuse fluorescence throughout the axon. Therefore, other methods of analysis were needed to determine their presence and movement patterns.

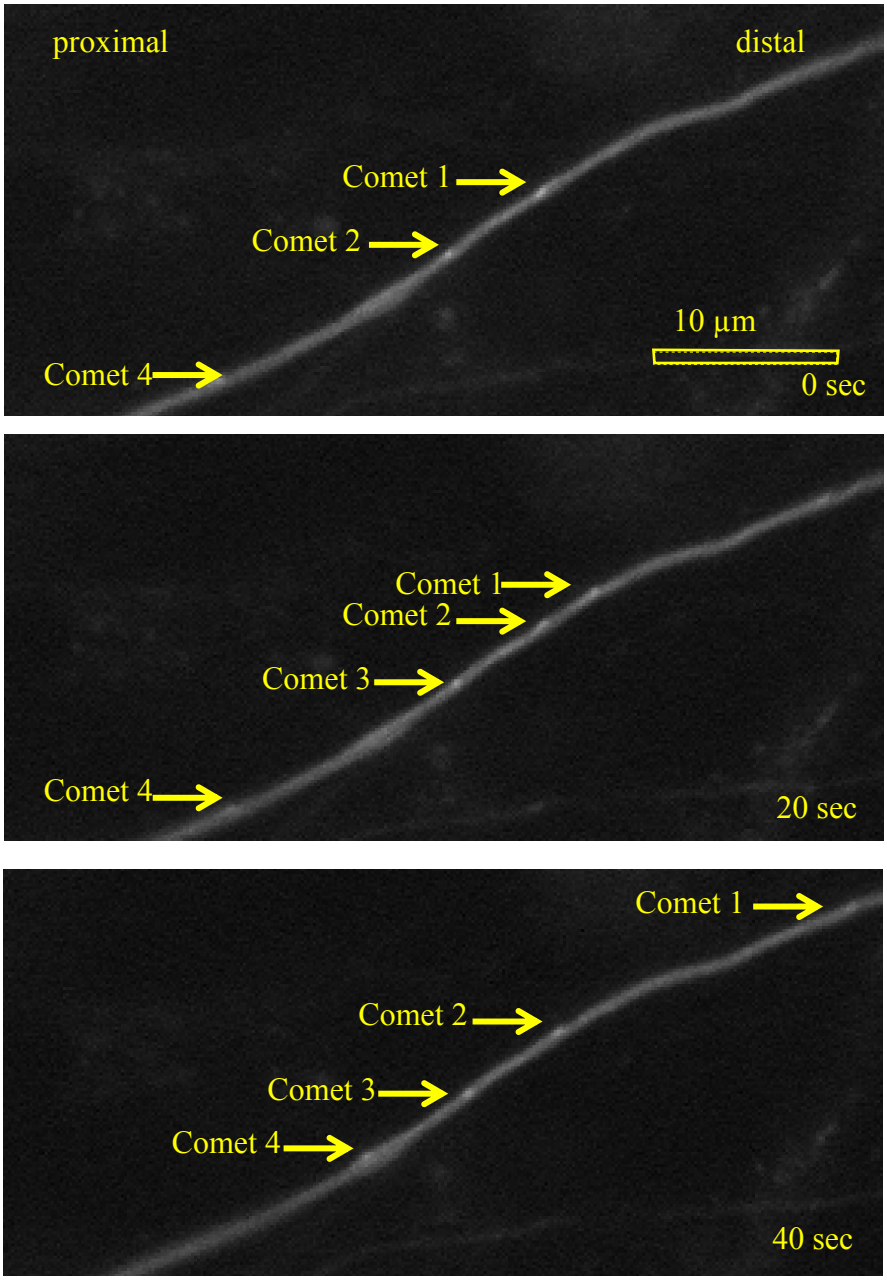

Figure 3.1: Visualization of EB3-mCherry comets through three frames from a movie. Yellow arrows indicate the position of each comet at each timepoint. Comet 1 pauses for a while and then moves. Comet 2 moves throughout the movie. Comet 3 comes into the focal plane after 10 sec. Comet 4 pauses for a while and then moves.

Because most comets were not easily visible by the human eye, a kymograph was used to assess their movement. A kymograph is a composite image that depicts the fluorescent intensity along the length of the axon per unit time. The y-axis of the image represents time and the x-axis represents a snapshot of the length of the axon for each frame of a time-lapse movie.

To create a kymograph, a kymograph-generating line was drawn along the length of the axon from left to right (or top to bottom). As shown in Figure 3.2 (top), the width of this line was set to encompass the entire axon. A horizontal row of pixels was generated at each timepoint, with each pixel representing a

pixel along the length of the line. This representative pixel possessed the maximum fluorescent intensity across the width of the line. The process was repeated for each frame of the movie (every 2 sec for 1-2 min) to yield the kymograph composite image (Figure 3.2, bottom).

Comets appeared as diagonal lines of fluorescent intensity in each kymograph, with the orientation of the line revealing the directionality of comet movement. A line from top left to bottom right indicated comet movement in the forward direction with respect to the direction in which the kymograph-generating line was drawn. This means that the line was drawn from the proximal to distal end of the axon (as shown in Figure 3.2). Conversely, comet movement in the reverse direction appeared as a line from the top right to the bottom left in the kymograph, indicating that the kymograph-generating line was drawn distal to proximal (not shown).

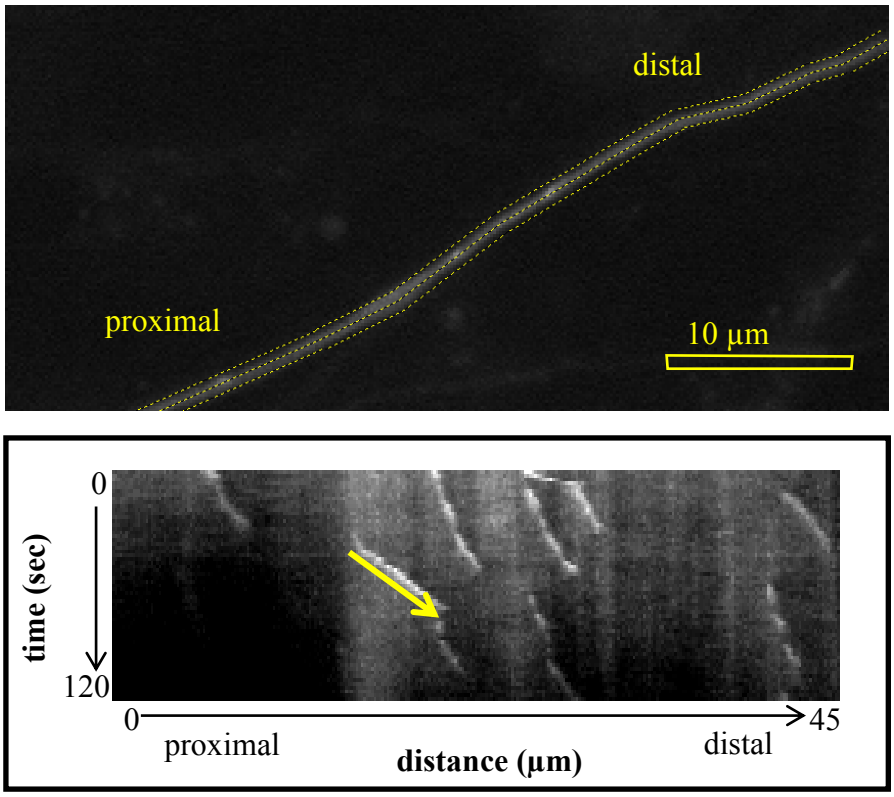

Figure 3.2: Generation of a kymograph using a kymograph-generating line that encompasses the length and width of the axon (top). The resulting kymograph (bottom) is a composite image with each horizontal row of pixels representing fluorescent intensity along the length of the axon at a single timepoint. The yellow arrow indicates the direction of movement of a comet.

Interpretability of EB3-mCherry Kymographs

In cells transfected with EB3-mCherry, there were considerable amounts of diffuse EB3-mCherry in the background. This diffuse fluorescence sometimes inhibited the ability to detect comets using a kymograph. Thus, prior to using the EB3-mCherry construct in conjunction with fluorescent photoactivation, it was necessary to ensure that interpretable kymographs could be obtained. If three or more comets were observed in a kymograph, and at least 90% of them were unidirectional, the

kymograph was considered "successful," or able to designate axon directionality. These criteria were based off of previous analysis showing that comets very rarely moved in the opposite (retrograde) direction (Stepanova, 2010; Wang, 2010).

It was desirable that at least one third of the axons exhibited successful kymographs. This would ensure that at least one third of transfected axons in a culture dish would allow for the use of EB3-mCherry in conjunction with fluorescent photoactivation. The EB3-mCherry construct exhibited a "success" rate of approximately 42% (15 out of 36 axons resulted in kymographs that matched the criteria). Therefore, the EB3-mCherry construct was deemed to be a fairly practical, although not ideal, method for designating axon directionality.

In order to improve this rate, a method for distinguishing "successful" axons prior to imaging was desired. Axons vary in thickness, and it is possible that in thick axons, comets may be less visible due to the contribution of out-of-focus fluorescence from diffuse EB3-mCherry. If thick axons yielded fewer detectable comets, it would be possible to select for thinner axons during the imaging process, ensuring that the kymographs obtained would be interpretable. Therefore, kymograph quality was examined in relation to axon width.

Figure 3.3 depicts the correlation between the number of comets in a kymograph as a function of axon width. The data did suggest the possibility of a negative correlation, as hypothesized, with thinner axons resulting in greater numbers of comets. However, the correlation was not strong and the relationship was not analyzed statistically.

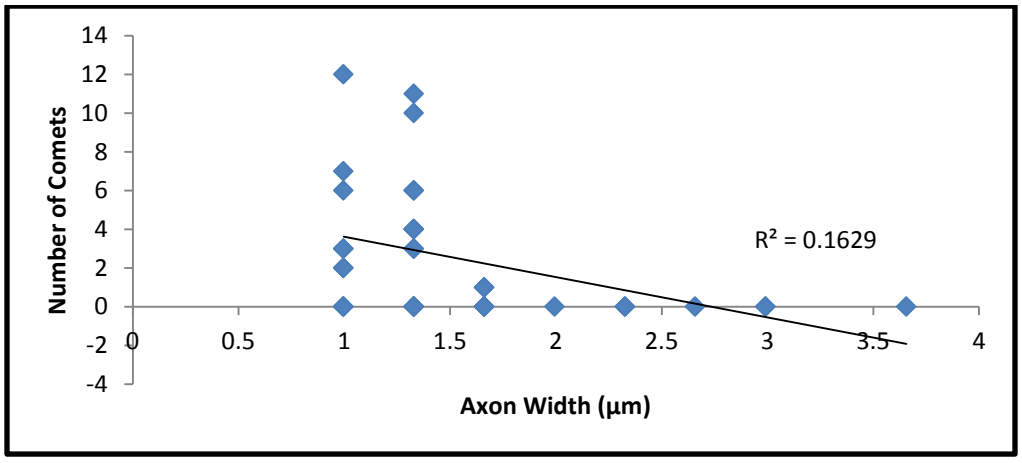

Figure 3.3: Correlation between axon width and number of comets using the EB3-mCherry construct. While data could suggest a possible trend with thinner axons resulting in greater comet visibility, the low coefficient of determination provided little support for this trend.

Comparison with EB1-YFP Construct

The EB3-mCherry construct was compared with another fluorescently-tagged EB protein construct, EB1-YFP, to determine whether kymograph success was dependent on the type of EB protein (EB3 versus EB1). The kymograph success rate for EB1 was similar to the EB3 construct, at 53% (8 out of 15 axons).

Figure 3.4 depicts the correlation between axon width and comet number for the EB1-YFP construct. Similar to the EB3 construct, a slight negative correlation was observed, but the correlation was not strong and statistical analysis was not conducted. Thus, the EB1 construct did not offer any improvement with respect to kymograph interpretability.

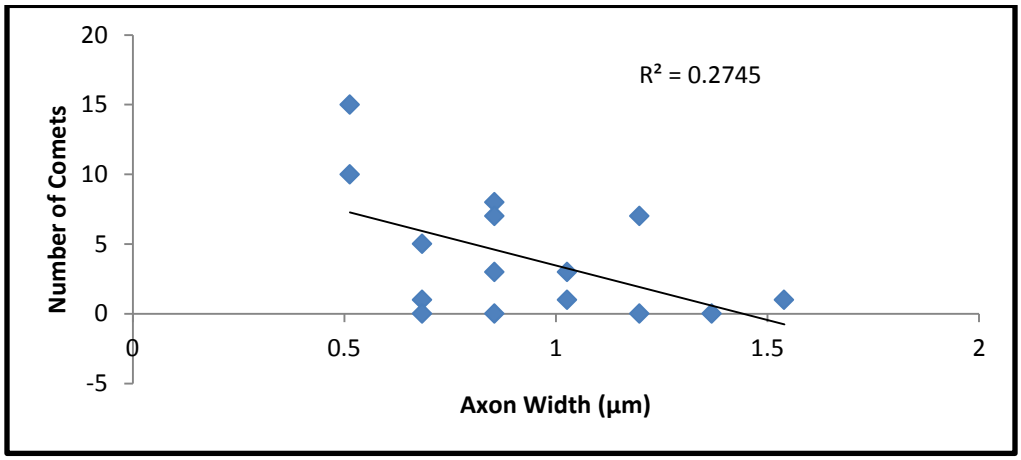

Figure 3.4: Correlation between axon width and kymograph comet number for the EB1-YFP construct. Results were similar to axons transfected with the EB3-mCherry construct.

Summary

- The purpose of this chapter was to examine the efficacy of using fluorescently-tagged EB proteins (which bind to growing tips of microtubules) to designate axon directionality with the hopes of adding a directionality component to the previously established "pulse-escape" technique.
- Areas of intense fluorescence, or comets, were detected in axons transfected with the EB3-mCherry construct. The direction of comet movement has been shown to accurately reveal the proximal and distal ends of each axon (Stepanova, 2010; Wang, 2010).
- Comet movement was monitored through the generation of kymographs (an image composite depicting a horizontal row of pixels for each frame of a time-lapse movie).
- Kymographs could not always detect comets because of considerable amounts of diffuse EB3-mCherry fluorescence throughout the axon. A kymograph was considered "successful" when greater than three comets were observed, with at least 90% of comets moving in the same direction.
- When using the EB3-mCherry construct, approximately 40% of kymographs were successful, and EB3-mCherry would therefore be useful in conjunction with fluorescent photoactivation.
- The EB3-mCherry construct was compared to the EB1-YFP construct to examine whether EB protein type affected kymograph quality. Results were similar between these two constructs.

Chapter 4: The Pulse-Spread Technique

Introduction

As previously discussed, the "pulse-escape" technique involved the use of a photoactivatable (PA) fluorescently-tagged neurofilament protein to observe trends in neurofilament transport (Trivedi, 2007). Acute activation ("pulse") of the PA fluorophore allowed for the detection of neurofilaments in the activated region (see Figure 1.8). Monitoring of fluorescent intensity in the activated region over time revealed trends in neurofilament movement out of the activated region ("escape").

The purpose of this study was to modify the previously established "pulse-escape" technique in order to determine directionality trends in neurofilament transport. In Chapter 3 of this thesis, the EB3-mCherry construct showed promise as a practical tool for determining the proximal and distal ends of an axon in rat DRG neuron-glial co-cultures. In this chapter, directionality designation using the EB3-mCherry construct is combined with the photoactivation of PA green fluorescent protein-tagged rat neurofilament M (PA-GFP-rNFM), resulting in the "pulse-spread" technique. Using this technique, one can observe not only the dispersal of neurofilaments from an activated region, but also the directionality of this dispersal ("spread"). This can allow for detection of anterograde or retrograde bias in neurofilament transport, an important component in overall neurofilament kinetics.

Demonstration of the Pulse-Spread Technique

One week after co-transfection with EB3-mCherry and PA-GFP-rNFM, neurons were imaged using the pulse-spread technique. First, mCherry fluorescence was detected and kymograph generation revealed proximal and distal ends of the axon. Then, a segment of axon approximately 30 µm in length was selected based on the criteria of being in focus and lacking background auto-fluorescent entities. This axon segment was divided into five regions of approximately 5 µm each. PA-GFP-rNFM was activated using violet light within the center region and GFP fluorescence was then captured at 0, 10, 20 and 30 min after activation.

Figure 4.1 depicts a representative cartoon of the pulse-spread technique alongside the pulse-spread images of an axon. Intense GFP fluorescence in the center region at 0 min indicated a successful activation. The spread of this fluorescence to the flanking regions over time was apparent, and indicated bidirectional neurofilament transport (in the axon depicted).

It is important to note that this spreading of fluorescence revealed the transport trends of a population of neurofilaments within an axon—individual neurofilaments may have been paused or moving at different speeds in different directions (as shown in the left panel of Figure 4.1). Because of the diffraction-limited resolution of a light microscope, individual neurofilaments could not be resolved in the fluorescence images. The uniqueness of the pulse-spread technique for observing neurofilament transport directionality lies in its ability to detect transport of neurofilaments at the population level in relatively neurofilament-rich axons (tens to hundreds of neurofilaments per cross-section).

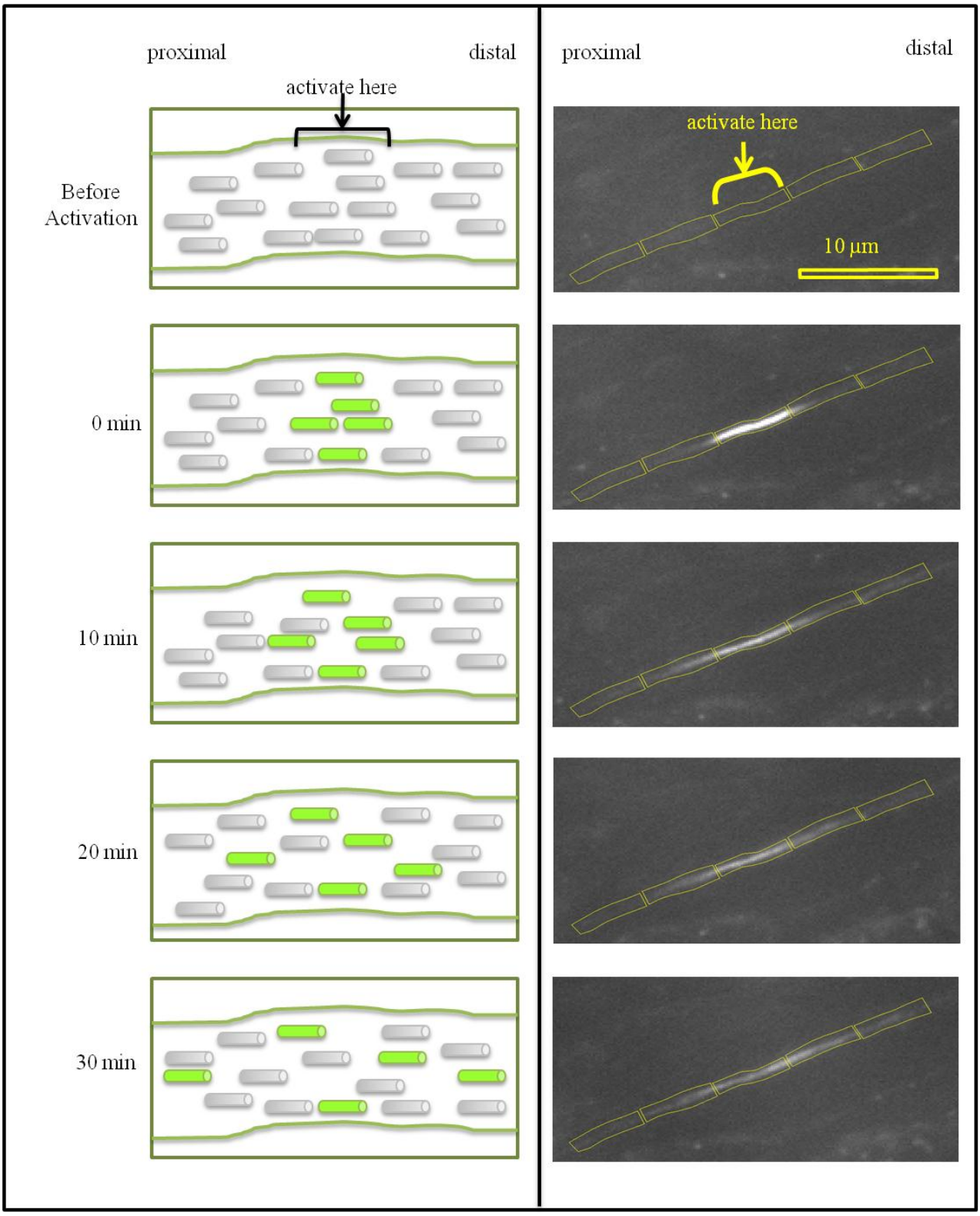

Figure 4.1: Cartoon representation of neurofilament activation and movement during pulse-spread imaging (left) alongside pulse-spread images of an axon (right).

Directionality of Neurofilament Transport

The integrated intensity of GFP fluorescence was obtained for each region of the axon at each time point for 11 axons using MetaMorph™ imaging software. Values were corrected for background fluorescence, auto-fluorescence and photo-bleaching, and then normalized to the intensity of activation.

Figure 4.2 shows scatter plots for each region with normalized fluorescence over time. The light gray lines indicate the average values for each time point. The activated region (CEN) displayed a trend similar to the double-exponential decay observed in previous "pulse-escape" studies (Alami, 2009; Trivedi, 2007). Previous experiments have also shown this departure to be dependent on glycolysis (Trivedi, 2007). The inner flanking regions (ANT1 and RET1) exhibited a marked rise in fluorescence, while further the outer regions (ANT2 and RET2) exhibited little change.

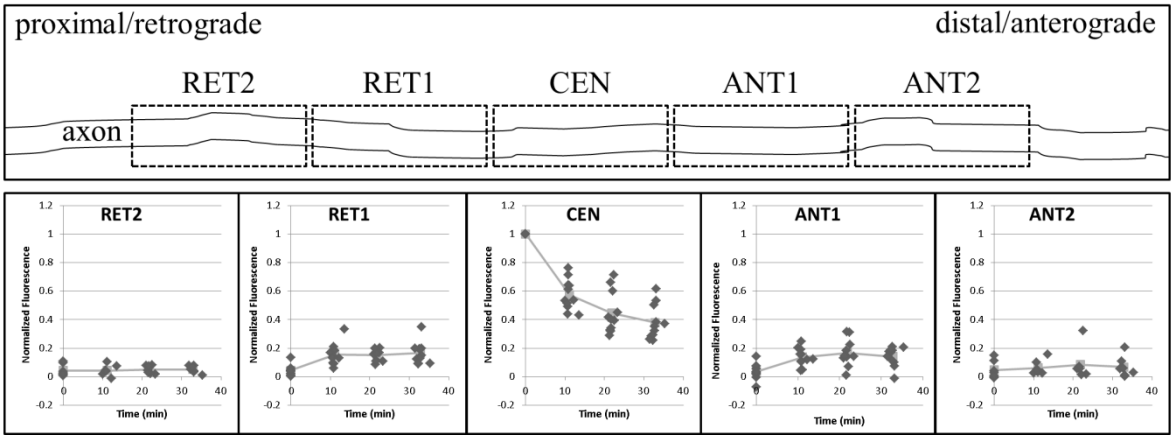

Figure 4.2: Schematic showing axon regions, with CEN being the activated region (top) alongside scatterplots depicting the change in fluorescence over time for each region (bottom).

Figure 4.3 shows this data in bar graph form, with the average normalized fluorescence in each region for each time point. A general spreading of fluorescence was observed over time. In the center activated region (CEN), the decrease in fluorescence was significant at each time point for the entire 30 min ($p < 0.01$). For the inner flanking regions (ANT1 and RET1), a significant rise was observed within the first 10 min ($p < 0.01$), with no significant change afterwards. The outer flanking regions (ANT2 and RET2) exhibited no significant changes in GFP fluorescence.

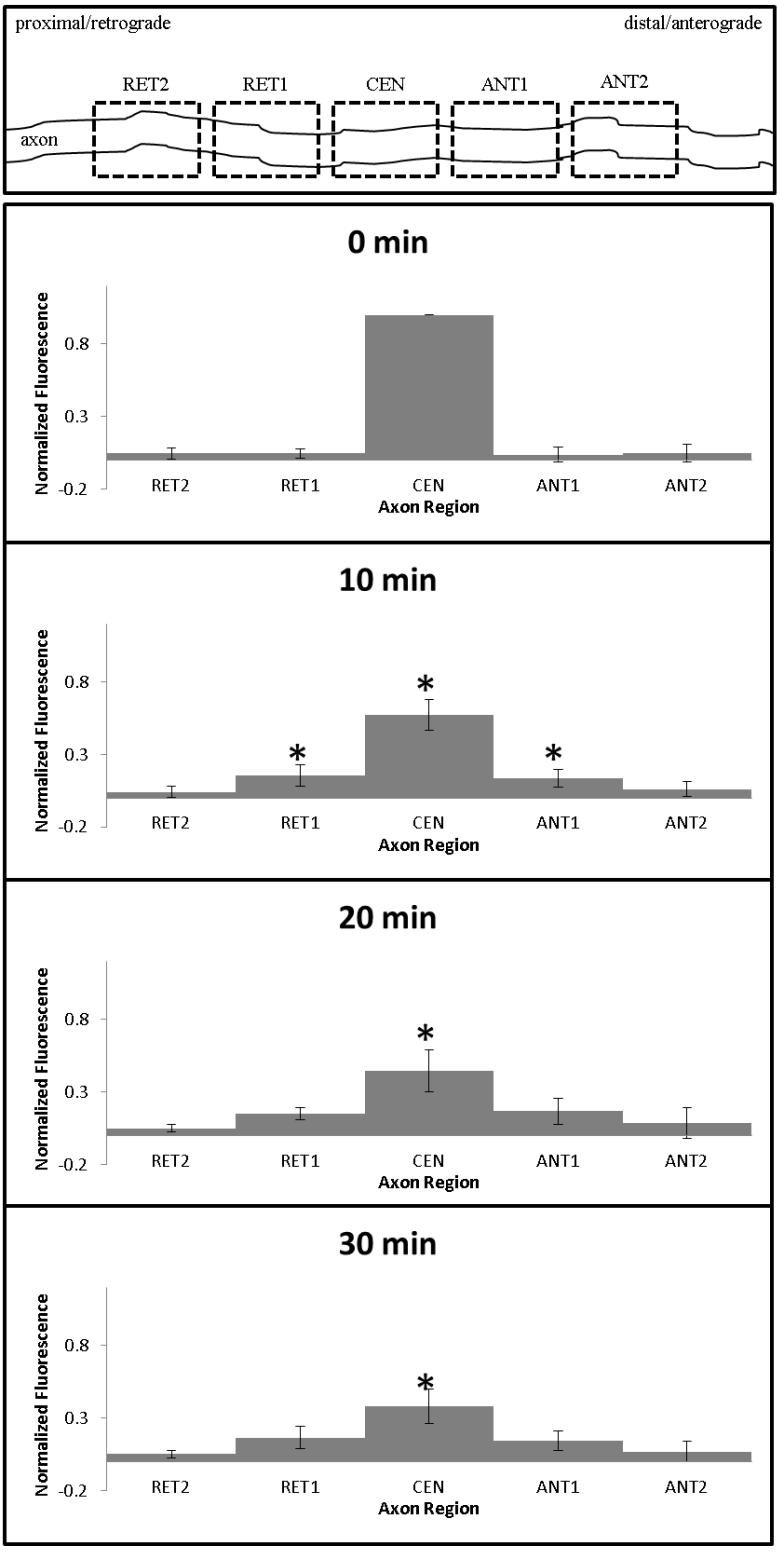

Figure 4.3: Bar graphs with average normalized fluorescent intensity in each region for each time point. Stars indicate significant difference ($p < 0.01$) in fluorescence between two time points within a single region. Schematic illustrating axon regions, with CEN being the activated region, included for reference (top).

It is important to note that significant retrograde transport was observed (RET1), indicating that neurofilament movement in these axons was bidirectional in nature. Amounts of anterograde and retrograde transport may have been similar in these axons, as no significant difference was found between them ($p > 0.5$). However, the large scatter in the data (observed in Figure 4.2) would have prevented any small, yet biologically important, differences between anterograde and retrograde transport from being observed.

The main cause for the large amount of scatter in the data was a low "signal-to-noise" ratio, resulting in possible inconsistencies during background correction. This was because activation fluorescence was relatively low compared to background fluorescence. In fact, activation fluorescence, averaging at approx. 330 afu (arbitrary fluorescence units), was only twice as strong as background fluorescence (approx. 170 afu on average). In an attempt to reduce background fluorescence, phenol Red-free NbActiv medium was used, which resulted in no apparent change. Thus, methods to increase activation fluorescence, as opposed to reduce background fluorescence, were considered (see below).

Increasing Efficacy Through Longer-Term, Myelinating Cultures

One method for increasing fluorescent signal is to increase the number of fluorophores present. This can be done through increasing the PA-GFP-rNFM transfection efficacy or increasing the total amount of protein present. Since transfection was already optimized for these cultures, increased neurofilament content was the next desirable solution to obtain more reliable pulse-spread data. Therefore, pulse-spread experiments were conducted on older, myelinating cultures, which were thought to be more neurofilament-rich. Although some axons in these cultures were myelinated, the ten axons on which pulse-spread was conducted were unmyelinated as before. Other than culturing technique and duration, methodology was identical to the previously discussed pulse-spread experiments on younger cultures.

Figure 4.4 shows scatterplots depicting the normalized fluorescence over time for each region for both younger, non-myelinating cultures (middle, same as Figure 4.2) and older, myelinating cultures (bottom). Compared to the younger cultures, older cultures exhibited a decrease in neurofilament dispersal from the activated region (CEN). Correspondingly, the rise of fluorescence in the immediate flanking regions (ANT1 and RET1) was dampened. This is consistent with the idea that neurofilament transport slows during axonal maturation (Griffin, 1985; Hoffman, 1983). It is important to note that the overall data exhibited slightly less scatter in these older cultures compared to the younger cultures. This may have been the result of a significant difference ($p < 0.05$) in activation intensity, with older cultures exhibiting over twice the amount of fluorescence at activation (approx. 790 afu compared to 330 afu). While there was less scatter in data obtained from older cultures, considerable variability still existed, as seen in Figure 4.4. Overall, older cultures resulted in brighter activation and less variability in the data, but this was counterbalanced by more pausing, resulting in no substantial improvement in the fluorescent intensity in the flanking regions.

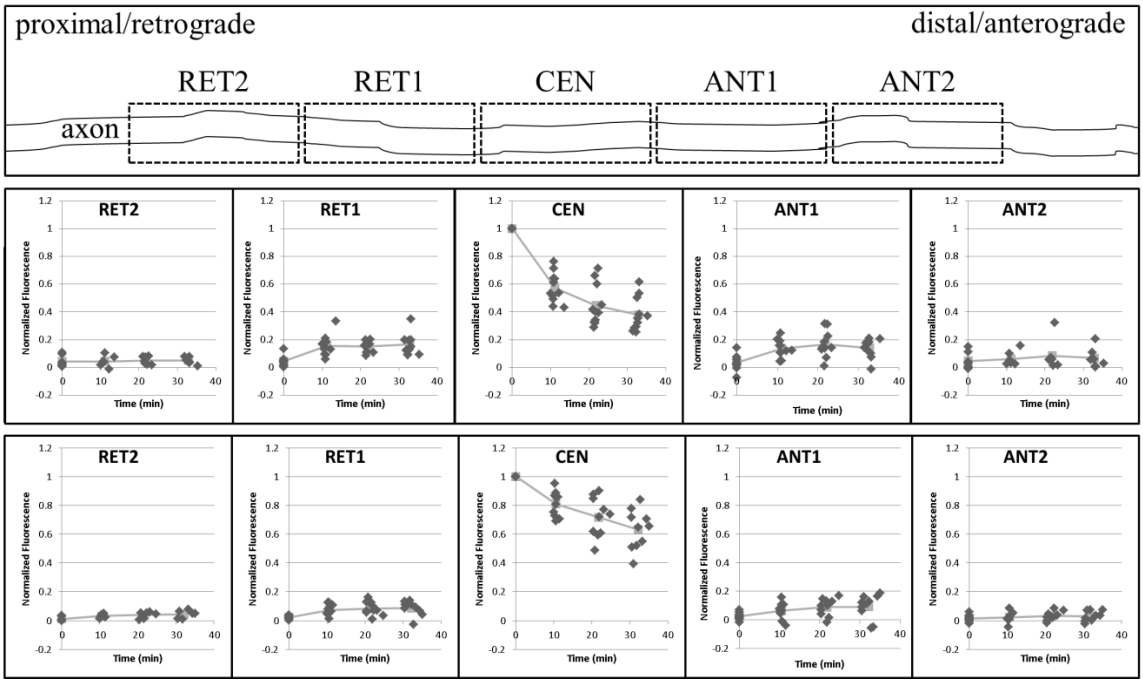

Figure 4.4: Scatterplots depicting normalized fluorescence over time for each axon region in younger cultures (middle) versus older cultures (bottom). Schematic of axon regions is included for reference (top).

Figure 4.5 shows this data in bar graph form, with average intensity in each region at each time point for younger cultures (left, same as Figure 4.3) versus older cultures (right). For both culture types, the decrease in fluorescence from the activated region was significant ($p < 0.01$) for the entire 30 min. Additionally, the rise in ANT1 and RET 1 fluorescence was significant ($p < 0.05$) for the first 10 min for both cultures. However, in the older cultures, ANT1 fluorescence continued to rise for 20 min, and RET2 fluorescence rose significantly ($p < 0.01$) in the first 10 min. This indicated that greater activation energy could result in a higher "signal-to-noise" ratio, allowing for the detection of previously hidden trends in neurofilament transport using the pulse-spread technique.

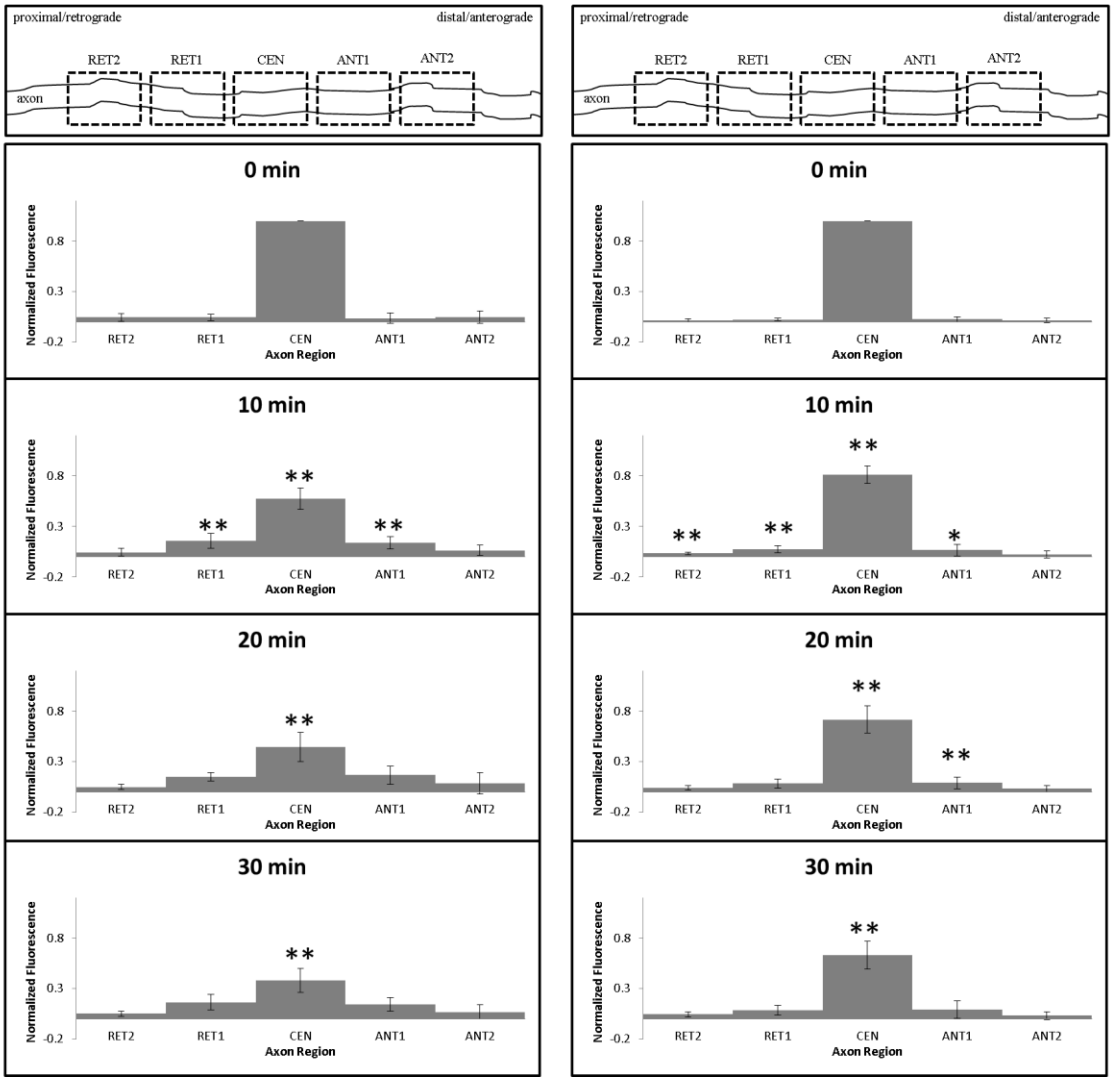

Figure 4.5: Bar graphs showing average normalized fluorescence in each axon region at each time point for young cultures (left) versus old cultures (right). Schematic of axon regions is included for reference (top). Stars indicate significant difference (*p < 0.05, **p < 0.01) in fluorescence between two time points within a single region.

Based on the symmetry of this data, it appeared that anterograde and retrograde transport were similar to each other. Table 4.1 depicts the average ratio (ANT1/RET1) at each time point for each culture type as well as the average percentage of ANT1 fluorescence compared to RET1 fluorescence. These data suggested the possibility of a slight anterograde bias (54-59% anterograde). However, high amounts of variability prevented any statistical differences from being detected, and therefore, specific conclusions could not be drawn.

Table 4.1: Ratio between ANT1 and RET1 fluorescence at each time point for young and old cultures as well as average percentage of ANT1 fluorescence compared to RET1 fluorescence.

Time (min)	Young Cultures (ANT1/RET1)	Old Cultures (ANT1/RET1)
10	1.2 ± 1.1	0.9 ± 1.0
20	1.2 ± 0.8	1.2 ± 1.6
30	1.1 ± 0.7	1.4 ± 1.3
% ANT1 on average	**59%**	**54%**
% RET1 on average	**41%**	**46%**

Although the neurofilament-rich axons of the older cultures resulted in greater activation intensity and decreased variability in the activated region, this was coupled with increased pausing, and therefore did not improve fluorescent signal in the flanking regions. Thus, the "signal-to-noise" ratio was not improved and variability prevented specific conclusions on anterograde versus retrograde bias from being drawn. Because age was most likely responsible for the increased pausing behavior resulting in low flanking fluorescence, alternate methods of obtaining more neurofilament-rich axons should be used. For example, using axons with greater inherent caliber, and therefore greater neurofilament content at all levels of maturity, would allow for the more precise detection of transport directionality.

Summary

- The purpose of this chapter was to describe the pulse-spread technique and evaluate its efficacy with the aims of examining the directionality of neurofilament transport.
- The photoactivated region exhibited significant decline in fluorescence over the course of 30 min, similar to previous "pulse-escape" experiments. Immediate flanking regions exhibited significant increase in the first 10 min, while further flanking regions exhibited no significant changes in fluorescence.
- A significant amount of retrograde transport was observed, indicating bidirectional movement of neurofilament within these axons. However, specific conclusions could not be drawn due to the high variability and low fluorescent signal.
- In order to increase fluorescent signal, and therefore reduce variability, older, myelinating, more neurofilament-rich cultures were used.
- In both culture types, the spread of fluorescence was broadly symmetrical, indicating similar amounts of transport in each direction. Comparison between the two directions of transport suggesting the possibility of a slight anterograde bias, but this difference was not statistically significant.
- In the older, myelinating cultures, a doubling of activation intensity was observed, along with reduction in variability. However, this was coupled with a decrease in transport, resulting in no improvement in flanking region fluorescence. Thus, reliable conclusions regarding anterograde or retrograde biases in neurofilament transport could not be drawn.

- The maturity of the axons in older cultures could account for the reduced transport (Griffin, 1985; Hoffman, 1983). Therefore, in order to obtain greater fluorescent signal, neurons with greater inherent neurofilament content (so as not to rely on age/maturity) should be isolated.

Chapter 5: NT-3 and Axon Caliber

Introduction

While the pulse-spread technique was viable, the data obtained was highly variable and difficult to analyze due to low fluorescent signal. As discussed in Chapter 4, an increase in axonal neurofilament content could resolve this problem, leading to greater confidence in the data obtained. First, neurofilament-rich axons would have increased amounts of the PA-GFP-rNFM construct, and therefore greater fluorescent signal. Additionally, by the Law of Large Numbers, an increase in neurofilament content would decrease the overall variability in the data, as a larger population of neurofilaments would be observed for each pulse-spread experiment.

This portion of the thesis describes the possible utilization of Neurotrophin-3 (NT-3) to select for a population of DRG cells that have higher neurofilament content with the hopes of obtaining greater signal for future pulse-spread experiments. Most laboratories that culture DRG neurons utilize nerve growth factor (NGF) as a component in culture medium, largely for historical reasons, as this was the first neurotrophic factor to be isolated. NGF was used for the experiments discussed in the previous chapters (see methods). However, studies have shown that different populations of neurons are responsive to different neurotrophins/growth factors. Specifically, DRG cells characteristic of smaller nociceptive neurons are NGF-dependent, while proprioceptive neurons, the largest sensory neurons, are NT-3-dependent (Snider, 1994; Snider, 1996). The large size of proprioceptive neurons is likely to be a result of greater neurofilament content, and indeed, NT-3 has been shown in to select for cells with more neurofilament-rich axons (Ip, 1993). Therefore, this experiment tested the promise of NT-3 to obtain axons better suited for the pulse-spread technique.

Visualization of Differences in Axon Caliber

DRG cells were cultured under myelinating conditions for 4 weeks in the presence of either NGF or NT-3. NGF cells were never exposed to NT-3 cells and vice versa, allowing for selection of either NT-3 or NGF dependent cells only. A fluorescent myelin stain was applied, which allowed for visualization of the myelin sheath as two parallel lines of fluorescent intensity, which indicated the edges of the axon. As seen in Figure 5.1, cells cultured in NT-3 exhibited different axonal morphology than those cultured in NGF. An apparent difference in size was observed, along with more kinks in axons cultured with NT-3. Additionally, NT-3 cultures were much less dense, indicating that fewer NT-3-dependent cells existed in the DRG compared to NGF-dependent cells. This is consistent with prior reports that the NT-3-dependent neurons are a smaller population of the DRG than the NGF-dependent neurons (Snider, 1996).

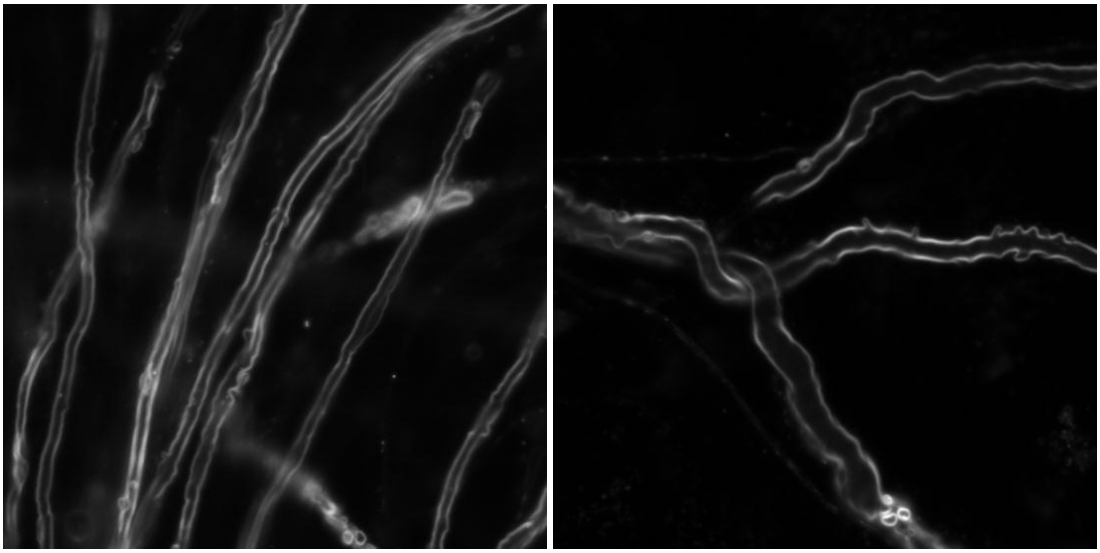

Figure 5.1: Representative images of axons of cells cultured for 28 days in the presence of NGF (left) and NT-3 (right).

Quantification of Differences in Axon Caliber

In order to quantify the difference in axon caliber between NGF and NT-3 cultures, a linescan profile method was used. Using the MetaMorph™ imaging software, a line was drawn perpendicular to each axon in a region that had smooth myelin, was well-focused, did not have uneven fluorescence in the background, and was representative of the rest of the axon.

A linescan profile was generated using a width of 10 pixels. This meant that for each pixel along the length of the line, the average intensity across the 10-pixel width was plotted. The resulting profiles displayed two peaks, one for the myelin sheath on each side of the axon. Figure 5.2 depicts an NT-3 axon with a perpendicular line and the resulting linescan profile. Two measurements of axon caliber were taken for each axon at half of the peak height, one for the inside of the myelin sheath and one for the outside.

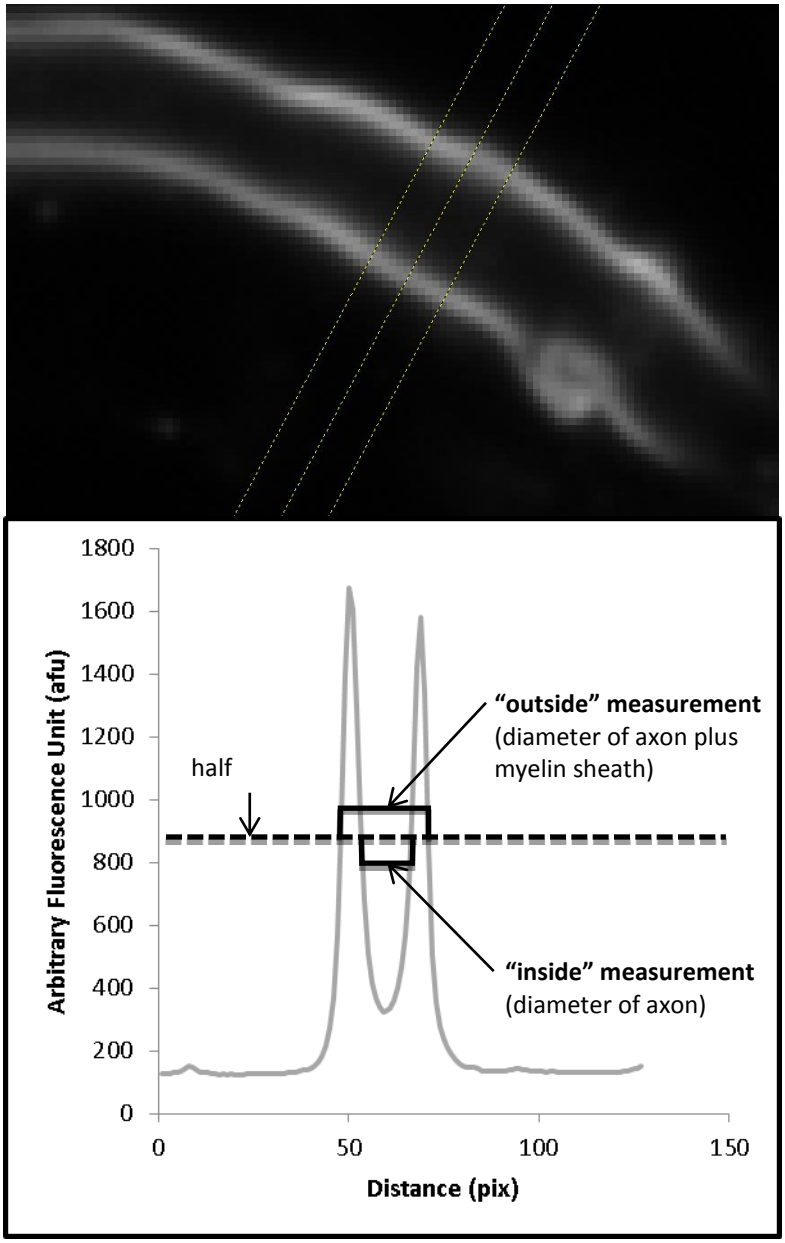

Figure 5.2: Depiction of linescan profile method of measuring axon caliber. A line perpendicular to the axon was drawn (top), and the average intensity was plotted for each pixel along the length of the line (bottom). "Inside" and "outside" measurements were taken to assess axon caliber.

"Inside" and "outside" measurements were then converted from pixels to micrometers for 30 axons in each culture condition. Because the myelin sheath hugs the axon tightly, the inside measurement corresponded to the axon diameter. Inside measurements were used to determine cross-sectional area assuming a circular cross-section, and were also subtracted from outside measurements to determine myelin thickness. Figure 5.3 shows the distributions for axon widths, as well as myelin thickness calculations. Distributions revealed greater heterogeneity in NT-3 cultures, with several axons that were larger than those in NGF.

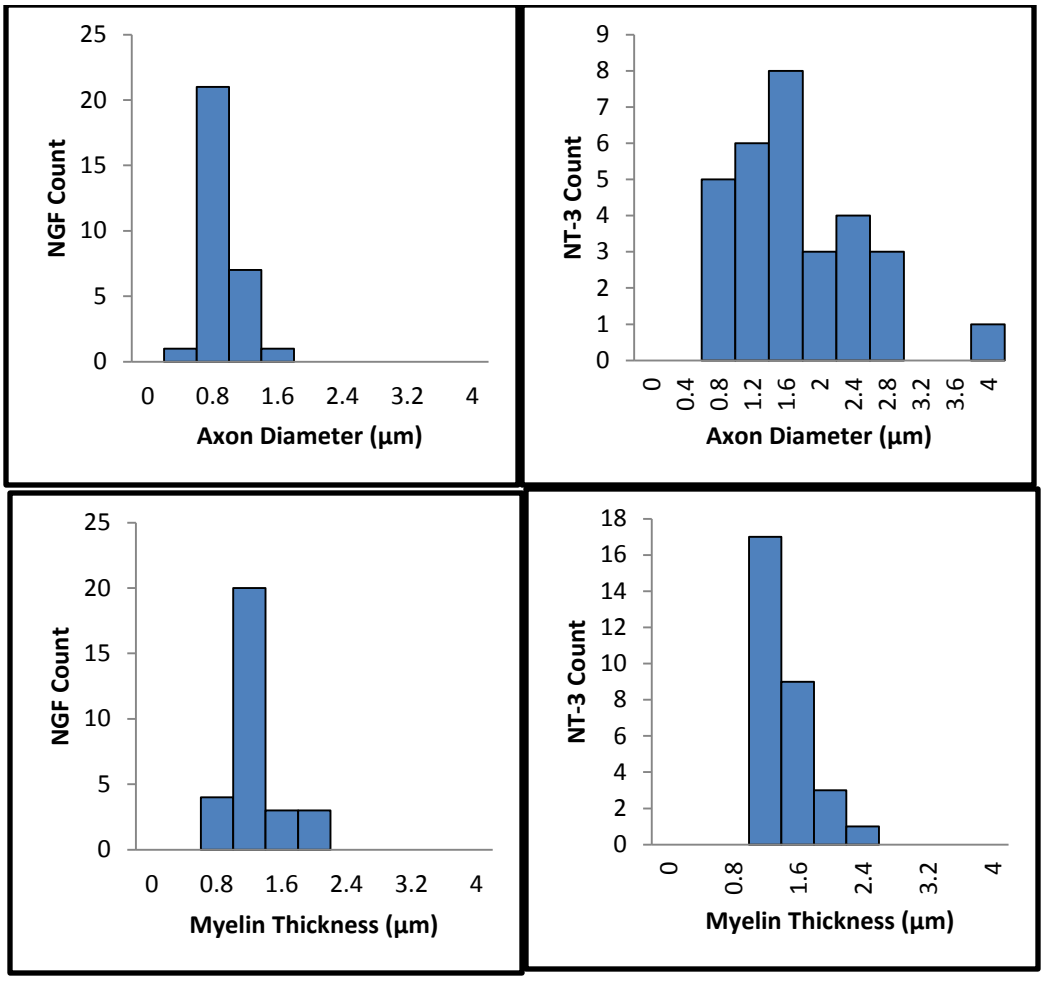

Figure 5.3: Distribution of axon diameter (top) and myelin thickness calculations (bottom) for NGF (left) and NT-3 (right) cultures.

Table 5.1 depicts the average values for measurements, calculated cross-sectional area, and calculated myelin thickness. Significant differences ($p < 0.01$) were observed between the two culture types for all values. Significance was determined using the Student's t-test, in which the two samples are assumed to have equal variance. However, the test has been shown to be highly robust regardless of variance when the samples are of similar size (Markowski, 1990), as they were in this experiment (n= 30 for each culture type). Additionally, the Student's t-test assumes a normal distribution, which was not apparent in all cases. Thus, in order to assess the validity of the t-test, a larger sample size may be required to discern the normalcy of distributions.

Table 5.1: Cross-sectional area and myelin thickness of axons as measured by linescan profile analysis.

	NGF	NT3
Outside Measurement (μm)	2.47 ± 0.33	3.56 ± 0.82**
Inside Measurement (μm)	1.03 ± 0.24	1.91 ± 0.72**
Calculated Cross-Sectional Area (μm^2)	0.87 ± 0.43	3.25 ± 2.56**
Calculated Myelin Thickness (μm)	1.45 ± 0.27	1.65 ± 0.31*
***p < 0.01, **p < 0.001**		

Interestingly, myelin thickness was slightly enhanced for NT-3 cultures (by approximately 110%). Although these observations contradict literature describing NT-3 inhibition of myelination (Shooter, 2010; Shooter, 2005; Chan, 2005; Shooter, 2001), they support a positive correlation between axon caliber and myelination (Dyck, 1985).

Quantification revealed that NT-3 axons had almost twice the caliber as NGF axons. The calculated cross-sectional area of axons in NT-3 cultures was approximately 370% greater than those in NGF cultures. If the neurofilament content was constant, as expected, this would suggest that NT-3 dependent cells had axons containing almost four times as many neurofilaments as NGF-dependent cells.

Summary

- The purpose of this experiment was to assess the potential of NT-3 over NGF in obtaining more neurofilament-rich axons, which would lead to greater PA-GFP-rNFM fluorescence for future pulse-spread experiments.
- Greater axon caliber was observed both qualitatively and quantitatively for NT-3-dependent cells as compared to NGF-dependent cells.
- Myelin thickness was slightly enhanced in NT-3 cultures, which may have been due to a balance between NT-3 inhibition of myelination and the positive correlation between axon caliber and myelination.
- Calculation of axonal cross-sectional area in NT-3 cultures suggested axons with 370% greater neurofilament content on average as compared to NGF cultures.
- Due to time constraints, neurofilament content differences were not confirmed through comparison of fluorescently-tagged neurofilament protein expression between the two cultures.
- Future studies on neurofilament transport should explore cell cultures supplemented with NT-3 instead of NGF, since NT-3 selects for cells with higher caliber axons that could result in almost four times as many neurofilaments. These cells do not grow in NGF-only culture.

Chapter 6: Discussion

Development of the Pulse-Spread Technique

In this study, the pulse-escape technique was successfully modified into the pulse-spread technique in order to analyze neurofilament transport directionality in DRG neurons. Development of the pulse-spread technique involved two phases. First, the EB3-mCherry construct was examined for its usefulness in determining the proximal and distal ends of an axon in DRG culture. Second, fluorescent photoactivation of PA-GFP-rNFM was conducted with the hopes of monitoring neurofilament transport directionality.

Phase 1: EB3-mCherry Utility

The EB3-mCherry construct resulted in diffuse fluorescence throughout the axon, as well as comets that designated the directionality within the axon. Interestingly, not all EB3-mCherry expressing axons exhibited comets. This may have been due to the presence of diffuse out-of-focus fluorescence, which interfered with the ability to distinguish the fluorescent intensity of the comets. Diffuse fluorescence could have been from soluble EB3-mCherry protein within the axoplasm, or from other comets that were not in the focal plane. In order to isolate the focal plane of interest when imaging comets, alternate imaging techniques, such as confocal microscopy, could be explored. However, it would be important to keep in mind that the diffuse fluorescence was useful for tracking the position of the axon in the second phase of pulse-spread. Overall, approximately 40% of axons yielded comets that could be appropriately analyzed to designate axon directionality. Therefore, the EB3-mCherry construct demonstrated utility in DRG cultures, and was thus useful for the pulse-spread technique.

Phase 2: Fluorescent Photoactivation

After designating directionality using the EB3-mCherry construct, excitation of the PA-GFP-rNFM construct was conducted. Activation was successful in most cases, and spreading of fluorescence was detectable. Data indicated similar amounts of anterograde and retrograde transport, but variability due to low fluorescent signal prevented specific conclusions from being drawn. Thus, provided that issues regarding low fluorescent signal are resolved in the future, the technique was proven to be successful overall.

Neurofilament Transport Directionality

A broadly symmetrical spread of the photoactivated neurofilaments was observed in DRG neurons, indicating that neurofilaments moved both in the anterograde and retrograde direction and that the amount of transport was similar in both directions. Statistical analysis showed no significant difference between the two directions of transport.

The data suggested substantial amounts of retrograde transport. Published measurements made by tracking single neurofilaments in low density cultures from various sources have yielded a range of proportions, from 54% anterograde in one study to 83% anterograde in another (Talbe 6.1). In this

study, pulse-spread measurements suggested a modest anterograde bias (54-59% anterograde), but there was too much variability to establish statistical significance. Since neurofilaments are synthesized and assembled in the neuronal cell body, an anterograde bias would be expected in axons, but more precise measurements would be required to prove if this was really the case.

Table 6.1: Results from previous studies observing single neurofilaments within low density cultures. Studies report varied amounts of retrograde transport. Percentages indicate number of neurofilaments moving in that direction.

Study	Method	Anterograde	Retrograde
Wang, 2010	Natural gap technique	54%	46%
Uchida, 2004	Imaging of distal axons 12-24 hrs after transfection	59%	38%
Wang, 2001	Transport through photobleached gaps	69%	31%
Wang, 2000	Natural gap technique	83%	17%

It is interesting that such a high degree of retrograde transport would be observed. At first glance, there seems to be no apparent advantage to the cell for expending energy on transport in both directions, and there is no current understanding in the field as to why this might be the case. One possible advantage for bidirectional transport could be its implication in neurofilament content and mechanisms of accumulation. The overall net velocity of neurofilament transport is a summation of anterograde, retrograde, and pausing rates. Thus, transport directionality affects the overall net velocity of neurofilaments, which in turn affects neurofilament residence time. Local decreases in neurofilament residence time would result in decreases in neurofilament content, while neurofilament accumulation would result from increases in residence time. Altering rates of reversal between anterograde and retrograde transport could be one mechanism of regulating net velocity, and therefore, residence time, which would then affect neurofilament content. For example, an anterograde:retrograde transport ratio of 55:45 would result in low net transport velocity. This would lead to higher residence time, and therefore greater neurofilament content. On the other hand, a ratio of 9:1 would result in a high net velocity, leading to a lower residence time and neurofilament content (Figure 6.1). Therefore, cellular signals may increase the fraction of neurofilaments moving retrogradely in order to slow neurofilament transport and modulate neurofilament distribution along axons.

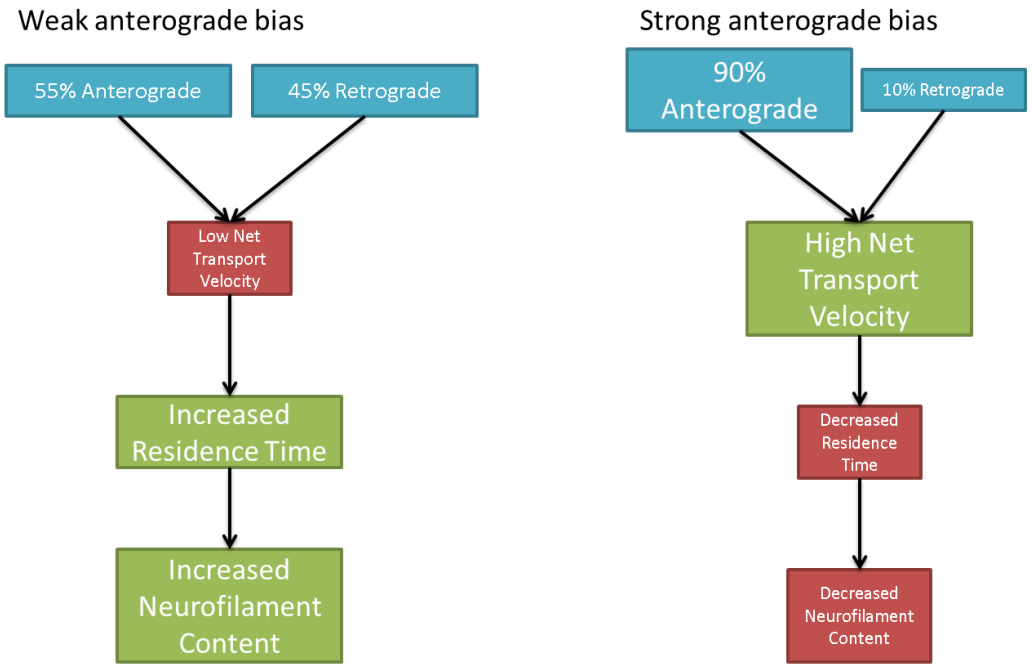

Figure 6.1: Schematic depicting effect of transport directionality on neurofilament content.

Challenges Involving Fluorescent Signal

While results suggested a slight anterograde bias, this difference was not statistically significant due to high variability in the data. Variability was most likely the result of camera noise from low amounts of detected signal from the flanking regions. Thus, increasing the amount of fluorescent signal could further enhance the power of the pulse-spread technique.

In the hopes of increasing fluorescent signal, older, myelinating cultures were used under the assumption that the axons in these cultures were more neurofilament-rich. Axons with greater neurofilament content would reduce variability because of an increase in sample size (neurofilaments per axon). Additionally, because more neurofilaments would be present, there would be a greater number of PA-GFP-rNFM fluorophores. The older, myelinating cultures were successful in increasing fluorescent signal at activation as well as reducing variability in the activated region. However, this was coupled with decreased transport, which was consistent with previous studies reporting decreased transport in older, more mature neurons (Griffin, 1985; Hoffman, 1983). This decrease meant that less neurofilaments moved outside of the activated region, resulting in no improvement of fluorescent signal in the flanking regions. Therefore, other mechanisms of obtaining neurofilament-rich axons would be needed.

Most investigators working with DRG cultures use NGF as a growth factor. However, NGF selects for a population of sensory neurons with the smallest axons, and therefore the lowest neurofilament content. In this study, culturing with NT-3 lead to neurons with larger axon calibers by almost 4-fold, which would indicate a proportional difference in neurofilament content. Due to time constraints, confirmation of

differences in neruofilament content was not conducted. Future studies should image axons after transfection with a fluorescently-tagged neurofilament protein construct so as to directly measure neurofilament content. Additionally, photoactivation after transfection with PA-GFP-rNFM will reveal whether NT-3 axons would have more efficacy in future pulse-spread experiments, and if this data would indeed be less variable in thicker axons.

In addition to increasing neurofilament content, other methods to increase fluorescent signal could also be examined. For example, utilization of brighter fluorescent protein constructs would reduce the "signal-to-noise" ratio when analyzing pulse-spread data. Additionally, more sensitive cameras would detect subtle differences in fluorescence that may not be detected otherwise. The ultimate goal of the pulse-spread technique is to determine the directionality of neurofilament transport in mature, neurofilament-rich axons, where single neurofilaments cannot be tracked. Thus far, the technique has successfully detected transport in these axons and revealed possible trends in transport bias. Future modification could further enhance this detection, making pulse-spread a promising method for the study of neurofilament transport directionality.

References

Akhmanova A and Steinmetz MO (2010). *Journal of Cell Science.* 123, 3415-3419.

Alami NH, Jung P, Brown A (2009). *The Journal of Neuroscience.* 29, 6625-6634.

Barry DM, Millecamps S, Julien JP, and Garcia ML (2007). *Experimental Cell Research*. 313, 2110-2120.

Beaulieu JM, Robertson J, and Julie JP (1999). *Cell Biology*. 77, 41-45.

Brown A (2000). *Nature Reviews: Molecular Cell Biology*. 1, 153-156.

Brown A, Wang L, and Jung P (2005). *Molecular Biology of the Cell*. 16, 4243-4255.

Chan JR, Cosgaya JM, Wu YJ, and Shooter EM (2001). *Proceedings of the National Academy of Science*. 93, 14661-14668.

Cosgaya JM, Chan JR, and Shooter EM (2002). *Science*. 298, 1245-1248.

de Vos KJ, Grierson AJ, Ackerley S, and Miller CCJ (2008). *The Annual Review of Neuroscience*.

de Waegh SM, Lee VMY, and Brady ST (1992). *Cell*. 68, 451-463.

Efimov A, Schiefermeier N, Grigoriev I, et al. (2008). *Journal of Cell Science*. 121, 196-204.

Eldridge CF, Bunge MB, and Bunge RP (1989). *The Journal of Neuroscience*. 9, 625-638.

Galjart N (2010). *Current Biology*. 20, R528-R537.

Glass JD and Griffin JW (1991). *The Journal of Neuroscience*. 11, 3146-3154.

Gold BG, Mobley WC, and Matheson SF (1991). *The Journal of Neuroscience*. 11, 943-955.

Gotow T (2011). *Cytoskeleton of the Nervous System*. Chapter 10. Ed. Nixon R and Aidong Y.

Gouveia SM and Akhmanova A (2010). *International Review of Cell and Molecular Biology.* 285, 1-74.

Hirokawa N, Niwa S, and Tanaka Y (2010). *Neuron.* 63, 610-638.

Hoffman PN, Griffin JW, Gold BG, and Price DL (1985). *The Journal of Neuroscience*. 5, 2920-2929.

Hoffman PN, Lasek RJ, Griffin JW, and Price DL (1983). *The Journal of Neuroscience*. 3, 1694-1700.

Julien JP (1997). *Trends in Cell Biology*. 7, 243-249.

Jung P and Brown A (2009). *Physical Biology*. 6, 046002.

Ip NY, Li Y, Yancopoulos GD, Lindsay RM (1993). *The Journal of Neuroscience.* 13, 3394-3405.

Li Y, Jung P, and Brown A (2012). *The Journal of Neuroscience.* 32, 746-758.

Liu Y and Ma Q (2011). *Current Opinion in Neurobiology*. 21, 52-60.

Markowski CA and Markowski EP (1990). *The American Statistician*. 44, 322-326.

Maurer SP, Founiol FJ, Bohner G, et al. (2012). *Cell.* 149, 371-382.

Patterson GH and Lippincott-Schwartz J (2002). *Science*. 297, 1873-1877.

Perlson E, Maday S, Meng-meng F, et al. (2010). *Trends in Neurosciences*. 33, 335-344.

Perrot R, Berges R, Bocquet A, and Eyer J (2008). *Molecular Neurobiology*. 38, 27-65.

Perrot R and Eyer J (2009). *Brain Research Bulletin.* 80, 282-295.

Snider WD (1994). *Cell*. 77, 627-638.

Snider WD and Silos-Santiago I (1996). *Philosophical Transactions of the Royal Society.* 351, 395-403.

Stepanova T, Smal I, van Haren J, et al. (2010). *Current Biology.* 20, 1023-1028.

Stepanova T, Slemmer J, Hoogenraad CC, et al. (2003). *The Journal of Neuroscience*. 23, 2655-2664.

Svenningsen AF, Shan WS, Colman DR, and Pedraza L (2003). *Journal of Neuroscience Research*. 72, 565-573.

Trivedi N, Jung P, and Brown A (2007). *The Journal of Neuroscience*. 27, 507-516.

Uchida A and Brown A (2004). *Molecular Biology of the Cell*. 15, 4215-4225.

Wang L and Brown A (2010). *Molecular Neurodegeneration*. 5, 1-13.

Wang L and Brown A (2001). *Molecular Biology of the Cell*. 12, 3257-3267.

Wang L, Ho C, Sun D, et al. (2000). *Nature Cell Biology*. 2, 137-141.

Watson DF, Glass JD, and Griffin JW (1993). *The Journal of Neuroscience*. 13, 4354-4360.

Windebank AJ, Wood P, Bunge RP, and Dyck PJ (1985). *The Journal of Neuroscience*. 5, 1563-1569.

Yamauchi J, Chan JR, Miyamoto Y, et al. (2005). *Proceedings of the National Academy of Science*. 102, 5198-5203.

Yamauchi J, Miyamoto Y, Tanoue, et al. (2005). *Proceedings of the National Academy of Science*. 102, 14889-14894.

Yan Y, Jensen K, and Brown A (2007). *Cell Motility and the Cytoskeleton*. 62, 299-303.

Yuan A, Rao MV, Sasaki T, et al. (2006). *The Journal of Neuroscience*. 26, 10006-10019.